AGU100 ADVANCING EARTH AND SPACE SCIENCE

JGR

Journal of Geophysical Research: Solid Earth

RESEARCH ARTICLE

10.1029/2018JB015689

Final Assembly of the Southwestern Central Asian Orogenic Belt as Constrained by the Evolution of the South Tianshan Orogen: Links With Gondwana and Pangea

Xin-Shui Wang[1,2,3], Reiner Klemd[3], Jun Gao[1,2,4], Tuo Jiang[5], Ji-Lei Li[1,2], and Sheng-Chao Xue[6]

[1]Key Laboratory of Mineral Resources, Institute of Geology and Geophysics, Chinese Academy of Sciences, Beijing, China, [2]Institutions of Earth Science, Chinese Academy of Sciences, Beijing, China, [3]GeoZentrum Nordbayern, Universität Erlangen-Nürnberg, Erlangen, Germany, [4]College of Earth Science, University of Chinese Academy of Sciences, Beijing, China, [5]Laboratory of Isotope Geochemistry, Wuhan Centre of China Geological Survey, Wuhan, China, [6]State Key Laboratory of Geological Processes and Mineral Resources, China University of Geosciences, Beijing, China

Key Points:

- The Wuwamen ophiolite formed in a mid-ocean ridge setting and got emplaced prior to ~440 Ma
- The formation of the Wuwamen ophiolitic mélange suggests that the final closure of the South Tianshan Ocean occurred at ~320 Ma
- The western Central Asian Orogenic Belt was not accreted to Gondwana prior to collision with Karakum–Tarim as part of Pangea at ~320 Ma

Supporting Information:

- Supporting Information S1
- Table S1
- Table S2
- Table S4
- Table S5
- Table S6
- Table S7
- Table S8
- Table S9
- Table S10
- Table S11

Correspondence to:
X.-S. Wang and J. Gao,
wangxinshui0716@mail.iggcas.ac.cn;
gaojun@mail.iggcas.ac.cn

Citation:
Wang, X.-S., Klemd, R., Gao, J., Jiang, T., Li, J.-L., & Xue, S.-C. (2018). Final assembly of the southwestern Central Asian Orogenic Belt as constrained by the evolution of the South Tianshan Orogen: Links with Gondwana and Pangea. *Journal of Geophysical Research: Solid Earth*, *123*, 7361–7388. https://doi.org/10.1029/2018JB015689

Received 24 FEB 2018
Accepted 16 JUL 2018
Accepted article online 25 JUL 2018
Published online 3 SEP 2018

Abstract The South Tianshan Orogen marks the final assembly of the southwestern Central Asian Orogenic Belt (CAOB) and the Karakum–Tarim cratons. Here we present an integrated mineralogical, geochemical, and geochronological study of the Wuwamen ophiolitic mélange in the South Tianshan to better understand the tectonic evolution of the western CAOB and its links to Gondwana and Pangea. Mantle peridotites with mineral compositions similar to those of abyssal peridotites and basalts with N-MORB geochemical affinities suggest that the Wuwamen ophiolite was formed in a mid-ocean ridge setting. Arc-related gabbro and plagiogranite stocks intruding the mantle peridotites yielded zircon U–Pb ages of 441.1 ± 4.2 and 442.8 ± 2.4 Ma, indicating that the Wuwamen ophiolite got emplaced prior to ~440 Ma. Sericite-quartz schist from the ophiolitic mélange matrix with abundant 481–319 Ma detrital zircon grains is crosscut by a two-mica granite dike with a zircon U–Pb age of 321.3 ± 1.7 Ma, thereby constraining the formation of the Wuwamen ophiolitic mélange at ~320 Ma. In conjunction with published data, we propose that the South Tianshan Ocean opened in the late Neoproterozoic and promoted the subsequent separation of microcontinents in the western CAOB from the northeast Gondwana margin during Gondwana assembly. Furthermore, the closure of the South Tianshan Ocean led to the final assembly of the southwestern CAOB and the Karakum–Tarim cratons and their incorporation into Pangea at ~320 Ma.

1. Introduction

The Central Asian Orogenic Belt (CAOB; Figure 1), located between the Baltica, Siberia, Karakum, Tarim, and North China cratons, underwent a long-lived geological evolution extending from late Neoproterozoic to early Mesozoic times, and witnessed the shaping of Gondwana and Pangea (Cawood & Buchan, 2007; Domeier & Torsvik, 2014; Han, Zhao, Cawood, et al., 2016; Sengör et al., 1993; Wilhem et al., 2012; Windley et al., 2007; Xiao et al., 2015). The final assembly of Gondwana was achieved by multiple orogenic events between 570 and 470 Ma, such as the Brasiliano Orogen, the North Indian Orogen, and the Ross-Delamerian Orogen (Cawood et al., 2007; Cawood & Buchan, 2007; Collins & Pisarevsky, 2005). Intriguingly, the western CAOB recorded coeval orogenic events, as indicated by the 530–470 Ma (ultra)high-pressure [(U)HP] metamorphism in the Kokchetav, Anrakhai, Aktyuz, Makbal, and Barleik metamorphic terranes (Figure 1; Alexeiev et al., 2011; Hermann et al., 2001; Klemd et al., 2015; Konopelko et al., 2012; Liu, Han, et al., 2016; Rojas-Agramonte et al., 2013). The Tarim and North China cratons bordering the CAOB to the north were thought to have been incorporated into northeast Gondwana based on the ~510–470 Ma (U)HP metamorphism along their southern margins (Han, Zhao, Cawood, et al., 2016; Metcalfe, 2013), which is in contrast with suggestions that both were unconnected with the Gondwana margin throughout the Paleozoic (Cocks & Torsvik, 2013; Wilhem et al., 2012). A pending issue however is whether the microcontinents (such as the Central Tianshan, Kazakhstan–Yili, and Kokchetav blocks) of the western CAOB had ever been integrated in East Gondwana, which is crucial to the architectural reconstruction of the CAOB.

The assembly of Pangea was completed by the end of the Triassic involving the progressively north directed migration of numerous terranes toward southern Siberia, including the CAOB units and the NE Gondwana-derived continental blocks which are now located in Southeast Asia (Domeier & Torsvik, 2014; Metcalfe,

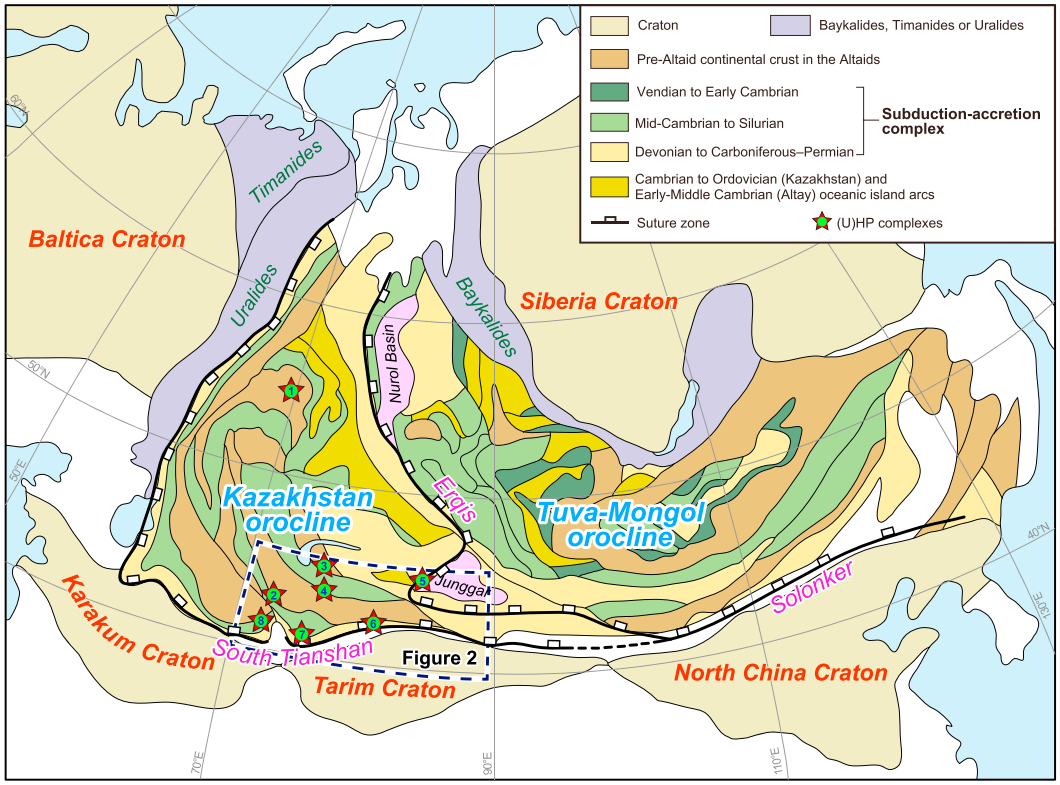

Figure 1. Tectonic map showing the main tectonic units of the Central Asian Orogenic Belt (modified from Sengör et al., 1993; Xiao et al., 2015). The (U)HP metamorphic rocks in the Kazakhstan Orocline are indicated by red stars, including (1) Kokchetav, (2) Makbal, (3) Anrakhai, (4) Aktyuz, (5) Barleik, (6) Akyazi, (7) Atbashi, and (8) Kassan.

2013; Stampfli et al., 2013). However, the exact time of docking of the Karakum–Tarim and North China cratons with the southern CAOB is highly disputed, which in turn leads to uncertainties concerning the timing of their integration into Pangea. Currently, final suturing of the western part of the southern CAOB was proposed to have occurred from late Devonian through Carboniferous to late Permian–mid-Triassic times (Charvet et al., 2011; Gao et al., 2011; Han et al., 2011; Han, Zhao, Sun, et al., 2016; Su et al., 2010; Wang et al., 2011; Xiao et al., 2015; Windley et al., 1990; Zhang et al., 2007), while termination of the Solonker suture zone in the eastern part was constrained to late Devonian or late Permian–mid-Triassic times (Eizenhöfer & Zhao, 2017; Xiao et al., 2015; Xu et al., 2013). Consequently, the exact final closure timing of the Paleo-Asian Ocean and the interaction of major tectonic units in the southern CAOB are critical for reconstructing the details of the Pangea assembly.

The South Tianshan Orogen in the southwestern CAOB (Figures 1 and 2) marks the welding of the Kazakhstan Orocline with the Karakum–Tarim cratons by closure of the South Tianshan Ocean (also known as Turkestan Ocean in the Kyrgyz Tianshan; e.g., Biske & Seltmann, 2010; Gao et al., 1998; Seltmann et al., 2011; Xiao et al., 2015). Yet some key issues remain rather speculative regarding the nature of the South Tianshan Ocean (a broad ocean versus back-arc basin), the subduction polarity of oceanic closure (southward versus northward versus bidirectional), and the timing of the final collision (e.g., Alexeiev et al., 2015; Charvet et al., 2011; Gao et al., 2009; Ge, Zhu, Wu, et al., 2012; Han & Zhao, 2017; Jiang et al., 2014; Klemd et al., 2015; Loury et al., 2015; Mühlberg et al., 2016; Safonova et al., 2016; Sang et al., 2018; Wang et al., 2011; Wang, Zhai, et al., 2017; Xiao et al., 2013). This is partly due to discrepancies in the interpretation of the nature and formation of the ophiolitic mélanges in the South Tianshan region (Figure 2) and their adaptation into the regional-scale tectonic evolution.

Ophiolites are interpreted as ancient oceanic lithosphere and are often emplaced along suture zones of fossil orogens that delineate major boundaries between assembled continental blocks or accreted terranes (e.g., Cawood et al., 2009; Dewey, 1976; Dilek & Furnes, 2011). However, ophiolites usually occur as

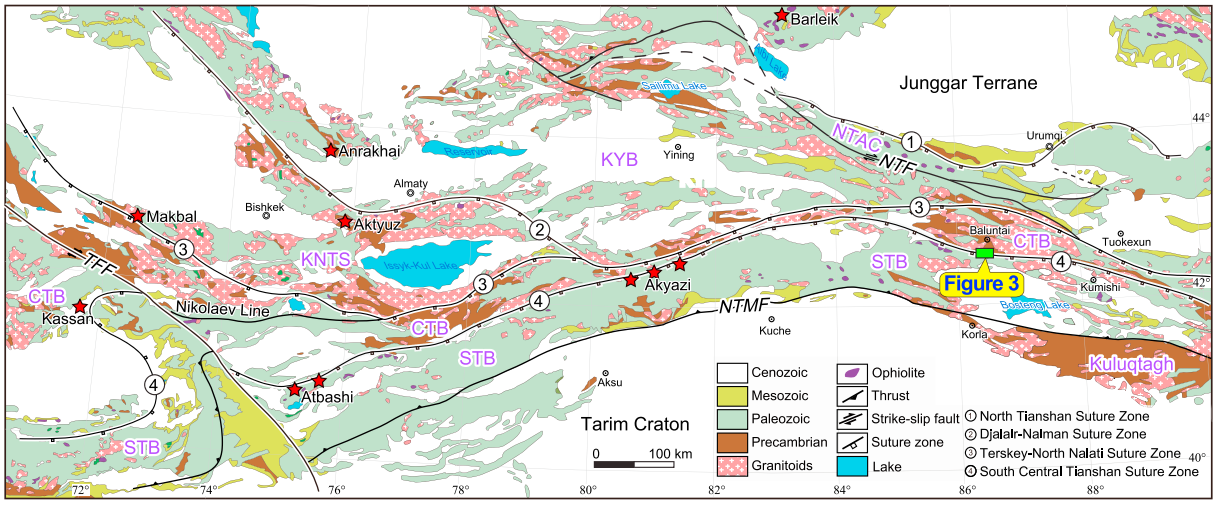

Figure 2. Geological map showing the tectonic subdivision of the Western Tianshan Orogen and adjacent areas in the southwestern CAOB (modified after Gao et al., 2009; Xiao et al., 2013; Wang, Gao, et al., 2017). The tectonic subunits include the North Tianshan Accretionary Complex (NTAC), the Kazakhstan–Yili Block (KYB), the Kyrgyz North Tianshan Block (KNTS), the Central Tianshan Block (CTB), and the South Tianshan Belt (STB). Major faults: NTF = North Tianshan Fault, NTMF = North Tarim Fault, TFF = Talas-Ferghana Fault. The locations of the (U)HP rocks are indicated by the red stars. The position of Figure 3 is marked.

dismembered fragments enclosed in chaotic mélanges and some of their units may be missing, which makes it difficult to define their formation ages. In addition, ophiolites form in various settings, such as mid-ocean ridges, marginal basins (back-arc or fore-arc), and continental margins (e.g., Dilek & Furnes, 2011, 2014; Miyashiro, 1973; Pearce, 2014). Thus, it is of paramount importance to pinpoint the precise nature of the ophiolites in the South Tianshan in order to link them with a single or several independent oceanic basins.

The present contribution includes field observations, mineral (i.e., olivine, pyroxene, and spinel) chemistry, zircon U–Pb–Lu–Hf isotope data, and whole-rock geochemistry of igneous and sedimentary rocks from the Wuwamen ophiolitic mélange of the South Tianshan, with the aim of constraining the nature and the timing of formation and emplacement of the Wuwamen ophiolite. In conjunction with published geological, stratigraphical, geochemical, and high-grade metamorphic data in the South Tianshan Orogen, the results provide new insight into the subduction-accretion and collision processes in the southwestern CAOB. We further show that the South Tianshan Ocean acted as a major barrier between the western CAOB and the Karakum–Tarim cratons during the Gondwana assembly and that the final assembly of the southwestern CAOB occurred at mid-Carboniferous (~320 Ma) times leading to the incorporation of the Karakum–Tarim cratons into Pangea.

2. Geological Setting

The South Tianshan Orogen formed as a result of a long-lasting interplay involving various terranes in the southwestern CAOB and the Karakum–Tarim cratons (Figure 2; e.g., Gao et al., 1998, 2015; Wang, Gao, et al., 2014; Xiao et al., 2013). In this study, the South Tianshan and adjacent areas are divided from north to south into the Kazakhstan–Yili Block (KYB), the Kyrgyz North Tianshan Block (KNTS), the Central Tianshan Block (CTB), the South Tianshan Belt (STB), and the Northern Tarim Craton (Figure 2; Wang, Gao, et al., 2014; Wang, Gao, et al., 2017).

The KYB, KNTS, and CTB are major units of the southern limb of the Kazakhstan orocline and are regarded as continental blocks welded by early Paleozoic acrretionary complexes (Kröner et al., 2012; Wilhem et al., 2012; Windley et al., 2007). The KYB is composed of a Neoarchean–Mesoproterozoic crystalline basement intruded by early Neoproterozoic (~926–845 Ma) gneissic granites and mid-Neoproterozic (~778–742 Ma) rift-related mafic dikes and felsic rocks (Kröner et al., 2007, 2012; Liu, Wang, et al., 2014; Wang, Liu, et al., 2014; Wang, Shu, et al., 2014). Overlying the basement are late Neoproterozoic sandstone, limestone and interlayered glacial diamictite, and Cambrian–early Ordovician phosphorous clastic-carbonate sequences on a passive continental margin (Ding et al., 2009; Gao et al., 1998; Wang, Shu, et al., 2014). Paleozoic

volcanic-plutonic rocks mainly show arc-related calc-alkaline affinities, which are associated with the subduction of the Junggar, Terskey, and South Tianshan oceans (e.g., Kröner et al., 2012; Long et al., 2011; Wang et al., 2018; Zhu et al., 2009).

The KNTS (also known as Kokchetav–North Tianshan or Stepnyak–Kyrgyz North Tianshan) is separated from the KYB by the Dajalair–Naiman suture zone defined by Cambrian–early Ordovician ophiolites and (U)HP metamorphic terranes (like Aktyuz and Anrakhai) and associated volcano-sedimentary rocks (Figure 2; Alexeiev et al., 2011; Klemd et al., 2014; Kröner et al., 2007, 2012; Ryazantsev et al., 2009; Rojas-Agramonte et al., 2013). The Precambrian rocks in the KNTS are poorly exposed with some metafelsic volcanic rocks yielding zircon U–Pb ages of 1373–1045 Ma (Kröner et al., 2013). The basement rocks are unconformably overlain by Cambrian to Carboniferous volcano-sedimentary successions (Bazhenov et al., 2003; Glorie et al., 2011). Voluminous Paleozoic magmatism mainly occurred during Cambrian–Silurian and Late Devonian–Early Permian times, and is related to the subduction and closure of the Terskey and South Tianshan oceans (e.g., De Grave et al., 2013; Glorie et al., 2010; Seltmann et al., 2011).

The CTB consists of the Kyrgyz Middle Tianshan (also referred to as Ishim–Middle Tianshan) and the Chinese Central Tianshan (Kröner et al., 2017; Qian et al., 2009; Windley et al., 2007). The tectonic boundary between the CTB and KNTS is marked by the Terskey–North Nalati suture zone that contains Cambrian to early Ordovician ophiolitic mélanges, UHP eclogite-facies rocks (i.e., Makbal), and associated turbidites (Klemd et al., 2015; Konopelko et al., 2012; Kröner et al., 2013; Lomize et al., 1997; Meyer et al., 2014; Qian et al., 2009; Rojas-Agramonte et al., 2013). Early Precambrian rocks in the CTB yielded Neoarchean to Paleoproterozoic ages (Kröner et al., 2017; Wang, Gao, et al., 2014; Wang, Gao, et al., 2017), and they are unconformably overlain by early Neoproterozoic siliciclastic rocks and limestones; late Neoproterozoic volcano-sedimentary rocks, dolomites, and glacial diamictites; and Cambrian to early Ordovician shallow-marine phosphorous clastic-carbonate formations (Levashova et al., 2011). In addition, a major angular unconformity was recognized between late Ordovician–early Devonian low-grade metavolcano-sedimentary successions and overlying late Devonian–Carboniferous unmetamorphosed volcanic rocks, terrigenous clastic sediments, and carbonates (Charvet et al., 2011; Gao et al., 1998; Wang et al., 2008). Widespread Neoproterozoic (~970–650 Ma) igneous rocks were presumably associated with the assembly and breakup of Rodinia (Gao et al., 2015; Konopelko et al., 2013, 2014). Intensive Paleozoic magmatism throughout the CTB is represented by Cambrian to Permian volcanic and intrusive rocks and interpreted to have formed during subduction-related, collisional, or postcollisional stages (e.g., Gao et al., 2009; Glorie et al., 2011; Konopelko et al., 2017; Long et al., 2011; Ma et al., 2012; Seltmann et al., 2011).

The STB is bounded by the South Central Tianshan Suture Zone (SCTSZ; also termed South Tianshan or Turkestan Suture) to the north and the North Tarim Fault to the south (Figure 2; Gao et al., 2009; Qian et al., 2009). The SCTSZ roughly runs from east to west along the Baluntai fault, the south Nalati fault, and the Atbashi–Inylchek fault, and continues along the south Ferghana fault to the west of the Talas–Ferghana fault. The suture zone is marked by discrete late Neoproterozoic to Carboniferous ophiolitic mélanges, (U)HP metamorphic terranes (i.e., Akyazi, Atbashi, and Kassan), and ocean plate stratigraphical elements (e.g., Alexeiev et al., 2015; Dolgopolova et al., 2017; Gao et al., 2009; Hegner et al., 2010; Jiang et al., 2014; Mühlberg et al., 2016; Safonova et al., 2016; Sang et al., 2018). However, some authors dispute that the Kyrgyz Middle Tianshan is the westward extension of the Chinese Central Tianshan and, instead, interpret the STB as its westward extension bounded by the south Nalati–Atbashi–Inylchek fault (also SCTSZ) to the north (Charvet et al., 2011; Wang et al., 2011; Wang, Zhai, et al., 2017). Alternatively, the STB was regarded as a broad fore-arc accretionary complex developed by a general southward accretion during northward subduction (Xiao et al., 2013). The STB consists mainly of imbricated late Ordovician to Carboniferous highly deformed clastic-carbonate successions with volcanic interbeds, which generally display a low- to medium-grade metamorphic overprint. Precambrian basement rocks are poorly exposed except the ~826–707 Ma granitic gneiss in the Muzaerte area and the Erbin Range (Alexeiev et al., 2015; Chen et al., 2000). Locally, the early strata are unconformably overlain by early Permian terrestrial volcano-clastic successions, interpreted to have been generated in a postcollisional setting (Huang et al., 2015; Liu, Guo, et al., 2014). Two phases of magmatism have been identified in the STB, which occurred at ~440–388 and 310–270 Ma, respectively (e.g., Huang et al., 2013; Konopelko et al., 2007; Lin et al., 2013; Seltmann et al., 2011; Zhao et al., 2015). In addition, a southern ophiolitic mélange belt is exposed in the south of the STB (see details in the next section; Han et al., 2011; Jiang et al., 2014; Han & Zhao, 2017; Wang, Zhai, et al., 2017).

The Northern Tarim Craton is characterized by a Neoarchean–Paleoproterozoic basement that is covered by Mesoproterozoic to early Neoproterozoic weakly metamorphosed marine clastic–carbonate sequences (Figure 2; e.g., Ge et al., 2013; Ge, Zhu, Wilde, Wu, et al., 2014; Lu et al., 2008; Zhang, Zou, et al., 2013). These rocks are unconformably overlain by late Neoproterozoic unmetamorphosed clastic rocks, glacial diamictites, bimodal volcanic rocks, and minor carbonates (e.g., Lu et al., 2008; Xu et al., 2009; Zhu et al., 2011). Paleozoic strata consist of Cambrian–Ordovician phosphorous siliciclastic and carbonate sequences, Silurian–Devonian shallow-marine clastic sediments, and Carboniferous–Permian clastic-carbonates and volcanic beds, which are separated by two major angular unconformities (Carroll et al., 2001; Han et al., 2015; Xiao et al., 2013). Several magmatic and tectonothermal events display Neoarchean to Permian ages, including ~830–790 Ma HP granulite-facies metamorphism (Ge et al., 2016; He et al., 2012), ~780–760 Ma Aksu blueschist-facies metamorphism (Yong et al., 2013; Zhang et al., 2012), and ~460–380 Ma arc-related plutonic rocks (Ge, Zhu, Wu, et al., 2012; Ge, Zhu, Wilde, He, et al., 2014).

3. The Ophiolitic Mélanges in the South Tianshan

Two ophiolite belts are exposed in the South Tianshan, i.e., a northern belt in the SCTSZ and a southern belt in the south of the STB. Up to now, two models have been suggested regarding the origins of the belts: (1) both are relics of one single normal oceanic basin (i.e., South Tianshan Ocean) whereby the southern belt represents allochthonous klippes that originated from the northern belt (Han et al., 2011; Han & Zhao, 2017; Xiao et al., 2013) or (2) relics of two separate oceanic basins, namely, a normal ocean basin (i.e., South Tianshan Ocean) and a back-arc or fore-arc basin from which the northern and southern belts were derived, respectively (e.g., Alexeiev et al., 2015; Charvet et al., 2011; Jiang et al., 2014; Wang et al., 2011; Wang, Zhai, et al., 2017). To the west of the Talas-Ferghana fault, the northern belt is defined by the North Ferghana, Karaterek, Sartale, Kan, North Nuratau, Teskuduk, and Bukantau ophiolitic mélanges (Alexeiev et al., 2015, 2016; Biske & Seltmann, 2010). Gabbros from the North Nuratau and Teskuduk ophiolites yielded zircon U–Pb ages of 448 ± 4 Ma (Mirkamalov et al., 2012) and 438 ± 6 Ma (Dolgopolova et al., 2017), respectively. In addition, fossils, such as radiolarians and conodonts, found in chert-rich sediments have ages ranging from early Ordovician to early Silurian times (Alexeiev et al., 2016; Biske & Seltmann, 2010; Dolgopolova et al., 2017). To the east, ophiolitic mélanges in the SCTSZ comprise the Aigyrbulak, Djanydjer, Changawuzi, Dalubayi, Guluogou, and Wuwamen ophiolites (Alexeiev et al., 2015; Han & Zhao, 2017; Jiang et al., 2014; Sang et al., 2018). Gabbros from the Djanydjer ophiolite in the Atbashi region revealed zircon U–Pb ages of 422–375 Ma (Sang et al., 2018; Wang et al., 2016), which are broadly consistent with early Devonian to early Carboniferous conodonts of the siliceous rocks (Alekseev et al., 2007). The age of the oldest ophiolite, the Dalubayi ophiolite, was determined by single zircon Pb–Pb ages of 600–590 Ma for gabbros and basalts (Yang et al., 2005). However, these ages are disputed (cf. Han, Zhao, Sun, et al., 2016). The gabbros of the Guluogou ophiolite, which occurs along the Baluntai fault, revealed zircon U–Pb ages of 334–332 Ma and were interpreted to have formed in a mid-ocean ridge (MOR) setting as evidenced by the close association with MORB- and OIB-type basalts (Jiang et al., 2014). More recently, however, the Wuwamen ophiolitic mélange—also exposed along the Baluntai fault—was dated at 334–309 Ma and interpreted to have originated in a short-lived back-arc basin (Dong et al., 2005; Wang, Zhai, et al., 2017).

The southern belt is defined by the Jigen, Baleigong, Qiqijianake, Misibulake, Madaleke, Aertengkesi, Kulehu, and Serikeyayilake ophiolitic mélanges. The Jigen ophiolite to the west of the Talas-Ferghana fault yielded a whole-rock Sm–Nd isochron age of 392 ± 15 Ma for MORB-type basalts (Xu et al., 2003). Cherty rocks from the Baleigong and Qiqijianake ophiolites of the Kokshaal area contain late Devonian to early Carboniferous radiolarians and conodonts (Han et al., 2011; Kang et al., 2010), while associated basalts revealed zircon U–Pb ages of 450 ± 2 Ma (Wang et al., 2007) and 399 ± 4 Ma (Wang et al., 2012). Further east, gabbros from the Misibulake, Mandaleke, and Aertengkesi ophiolites in the Heiyingshan area yielded zircon U–Pb ages of 425–392 Ma, and in addition, late Devonian–early Carboniferous radiolarians and conodonts were identified in siliceous sediments (Han et al., 2011; Jiang et al., 2014; Wang et al., 2011). Mafic rocks from the ophiolites show complex geochemical signatures with N-MORB, E-MORB, OIB, and arc affinities, thereby suggesting that these rocks were formed in a suprasubduction zone (SSZ) setting of a back-arc or fore-arc basin (Jiang et al., 2014; Wang et al., 2011). The gabbros of the Kulehu ophiolite revealed zircon U–Pb ages of 425–418 Ma, while N-MORB-type basalts and associated mid-Devonian to early Carboniferous radiolarians in cherts suggest an origin in a small oceanic basin (Liu et al., 1994; Long et al., 2006; Ma et al., 2007). A gabbro of the

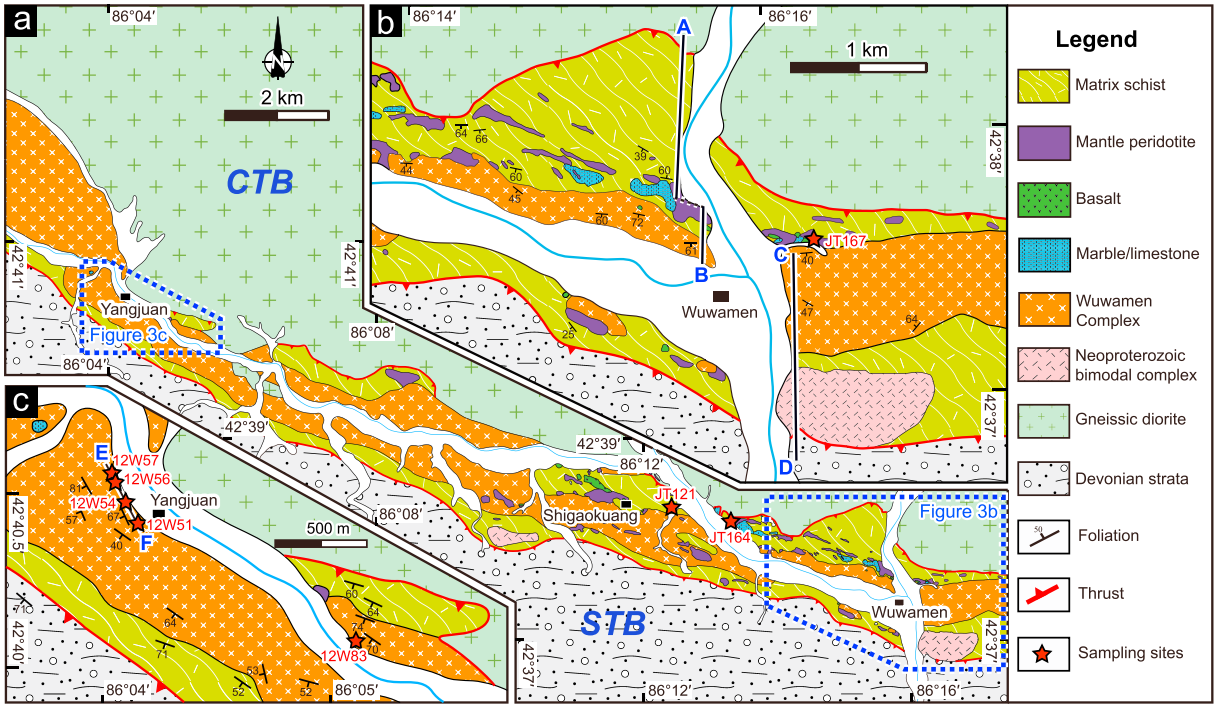

Figure 3. Geological map of the Wuwamen area, south of Baluntai, showing the Wuwamen ophiolitic mélange between the Central Tianshan Block (CTB) and the South Tianshan Belt (STB) with a typical block-in-matrix structure. Locations of cross sections and samples are denoted.

Serikeyayilake ophiolite has a zircon U–Pb age of 423 ± 10 Ma and was thought to have formed in a SSZ setting based on the presence of SSZ-type mantle peridotites and N-MORB-type basalts (Jiang et al., 2014). Notably, the Yushugou granulite terrane with a presumed ophiolite affinity (Jiang et al., 2014; Wang et al., 2011; Wang, Zhai, et al., 2017; Yang et al., 2011) in the Kumishi area was reinterpreted as continental arc root rocks overprinted by multiphase metamorphism during 398–322 Ma (Jian et al., 2013; Zhang et al., 2018; Zhang & Jin, 2016).

The here studied Wuwamen ophiolitic mélange, extending NWW-SEE with a width of about 2 km, is exposed along the Baluntai fault, which juxtaposes against the CTB to the north and the STB to the south (Figures 3 and 4; Dong et al., 2005; Wang, Gao, et al., 2014; Wang, Gao, et al., 2017). The CTB is overthrust by the southern Wuwamen ophiolitic mélange and mainly represented by a suite of highly deformed early Paleozoic (475–416 Ma) gabbro and diorite batholiths formed in a continental arc setting (Ma et al., 2012; Zhong et al., 2015). Approaching the contact zone, the tightly folded mélange displays a subvertical foliation due to intensive mylonitization. The batholiths were also strongly mylonitized with a south dipping foliation defined by oriented hornblende and plagioclase, indicating a top-to-the-north thrusting (Figure 4). To the south, the STB is separated from the Wuwamen ophiolitic mélange by a south dipping fault (Figures 3 and 4). The STB is dominated by shallow-marine sequences that contain sandstones, calcareous mudstones, and limestones, which were variably deformed and overprinted by greenschist-facies metamorphism. This stratigraphic sequence shows pervasive south or southwest dipping foliations with gentle to subhorizontal stretching lineations (Figure 4a) and south vergent overturned folds, indicating top-to-the-north thrusting and subsequent dextral shearing (this study; Wang, Zhai, et al., 2017).

The Wuwamen ophiolitic mélange mainly consists of allochthonous tectonic fragments of mylonitized marine sedimentary rocks, limestones/marbles, Precambrian basement, and ophiolitic slices in a chaotic matrix of late Paleozoic turbidites (Figures 3 and 4). Both the fragments and the turbiditic matrix exhibit broadly uniform south dipping foliations and gentle to subhorizontal stretching lineations (Figures 3 and 4), further indicating top-to-the-north thrusting and subsequent dextral shearing. Our recent studies revealed that the Precambrian fragments consist mainly of Neoarchean to Paleoproterozoic (~2.5–1.7 Ga) amphibolite-facies supracrustal assemblages (i.e., the Wuwamen Complex in Figure 3) and a Neoproterozoic (~790–730 Ma) bimodal complex, which were thought to represent basement rocks that

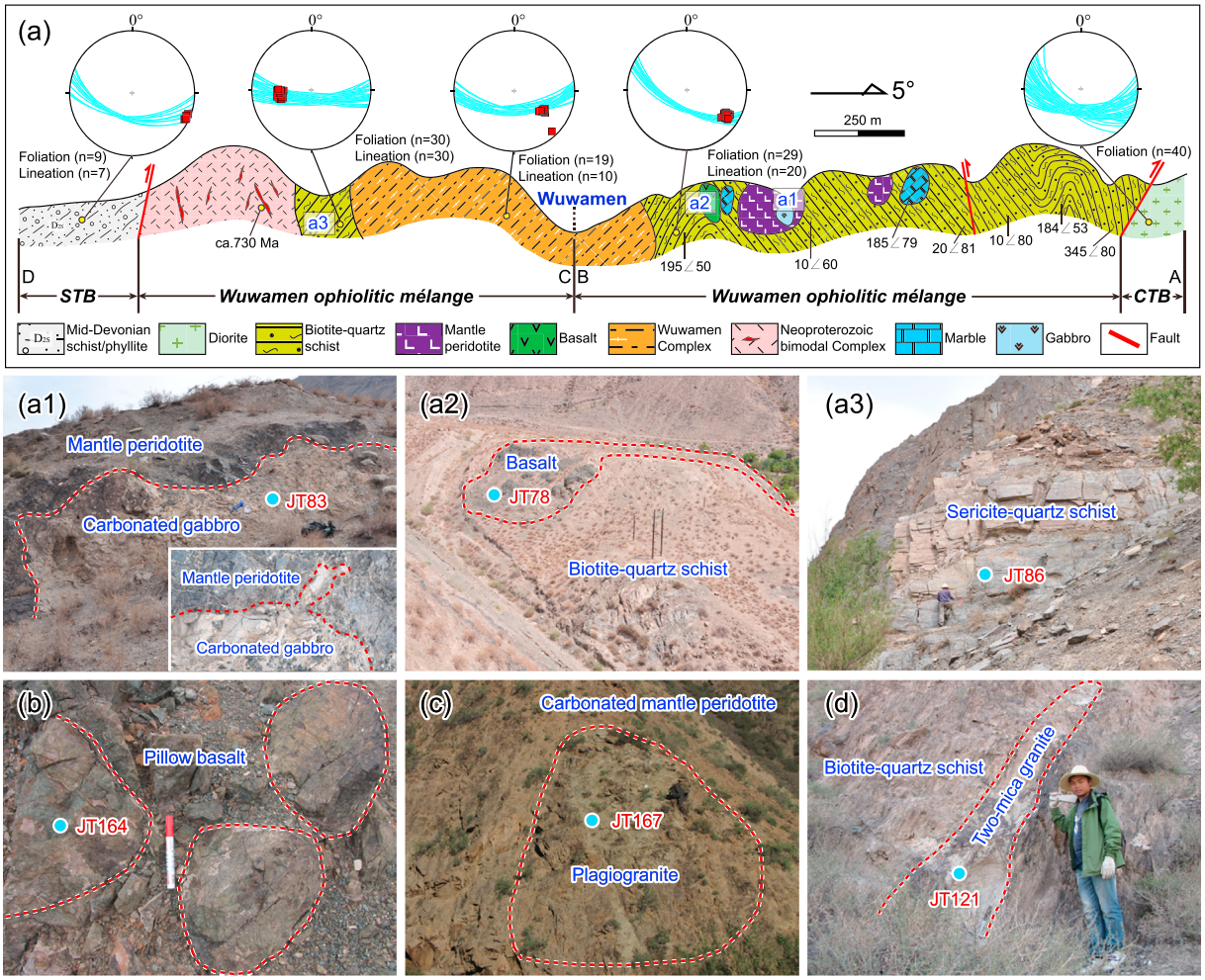

Figure 4. (a) Geological cross section (AB-CD) covering the Central Tianshan Block (CTB), the Wuwamen ophiolitic mélange, and the South Tianshan Belt (STB) from north to south. Note that the consistent orientations of the foliations and lineations in the inset lower hemisphere Schmidt plots are observed in the different lithotectonic units, indicating the overprint of NE-SW thrusting and NW-SE ductile strike-slip shearing. (a1) A carbonated gabbro stock (JT83) intruding the serpentinized mantle peridotite. (a2) Basalts (JT78) enclosed as blocks in the biotite-quartz schist matrix. (a3) A sericite-quartz matrix schist (JT86) displaying south dipping foliations. (b) Well-preserved pillow structures in the basalt blocks (JT164). (c) A plagiogranite stock (JT167) intruding the carbonated mantle peridotite. (d) A two-mica granite dike (JT121) crosscutting the biotite-quartz schist matrix.

were scrapped off the CTB during Paleozoic subduction-accretion (Gao et al., 2015; Jiang et al., 2015; Wang, Gao, et al., 2014; Wang, Gao, et al., 2017). The ophiolitic tectonic slices include strongly foliated mantle peridotites, basalts, and cherts, whereas gabbros and sheeted dikes have not been identified yet (Figures 3 and 4). Recently, OIB-like andesites with a zircon U–Pb age of 309 ± 4 Ma were interpreted as ophiolitic components; however, they show arc signatures and highly evolved Nd isotopic compositions ($\varepsilon_{Nd}(t) = -11.2$ to 0.5; Wang, Zhai, et al., 2017). Field observations show that the mantle peridotites underwent pervasive serpentinization and/or carbonatization and are locally crosscut by small gabbro and plagiogranite stocks (Figure 4). The variably folded and sheared matrix of mainly biotite-quartz schists was intruded by several (deformed) granitic dikes (Figure 4; this study; Wang, Zhai, et al., 2017). In addition, several granitic dikes and/or sills intruded the Precambrian fragments in the Yangjuan area, to the northwest of the ophiolitic mélange (Figures 3 and 5).

4. Analytical Methods and Results

Spinel, olivine, and pyroxene of the mantle peridotites were analyzed for their chemical compositions and the basalts for whole-rock element and Sr–Nd isotopic compositions in order to determine the precise nature and

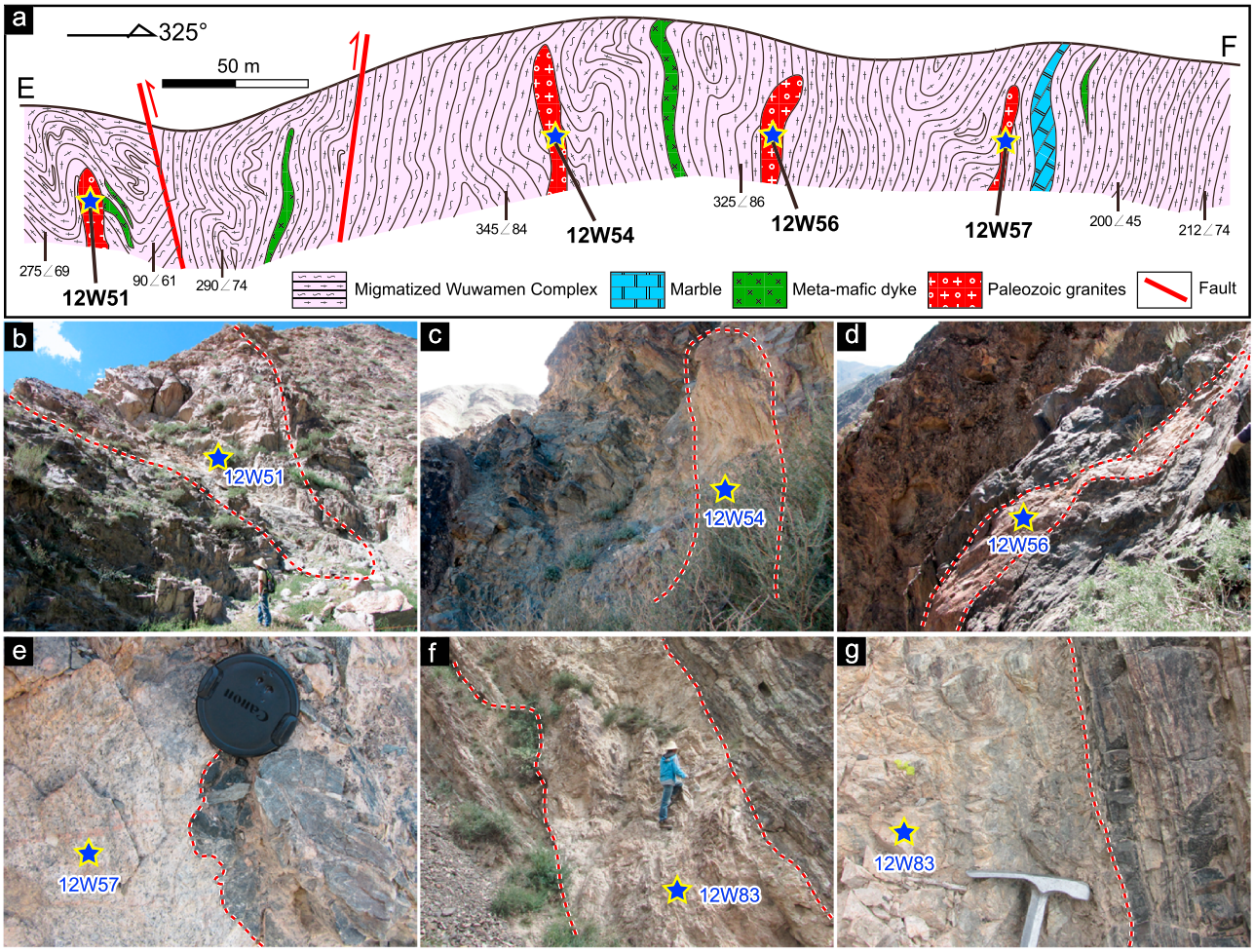

Figure 5. Geological cross section EF (as denoted in Figure 3c) and selected field photos illustrating the Paleozoic granitic sills and/or dikes (12W51, 54, 56, 57, 83) intruding the migmatized Wuwamen Complex with protolith formation ages of ~2.5 Ga (Wang, Gao, et al., 2017) in the Yangjuan area.

tectonic setting of the Wuwamen ophiolite. The gabbro and plagiogranite stocks intruding the mantle peridotites were collected for SIMS and LA-ICP-MS zircon U–Pb dating and Hf isotopic analyses with the aim of obtaining a minimum age for the ophiolite emplacement. Furthermore, sericite-quartz schist of the ophiolite mélange and one crosscutting two-mica granite dike were sampled for zircon U–Pb dating in order to constrain the lower and upper formation age limits of the ophiolitic mélange, respectively. In addition, five granitic sill and/or dike samples from Precambrian fragments were taken for zircon U–Pb dating and whole-rock geochemical analyses in order to place constraints on the tectonic evolution of the Wuwamen ophiolitic mélange. Details of the analytical procedures are described in the supporting information S1, and the analytical data are summarized in Tables S1–S7.

4.1. Mineral Chemistry of the Mantle Peridotites

The mantle peridotites were affected by intensive mylonitization and alteration, which commonly obscure the primary magmatic texture and mineralogy. In places, relics of olivine, clinopyroxene, orthopyroxene, and spinel were recognized in the relatively fresh peridotites (Figure S1). Five peridotite samples (JT26–1, –2, –4, –6, and JT104–7) were chosen for mineral analyses, and the chemical data are listed in Table S1. Olivines have high forsterite (Fo = 89.8–91.1) contents with 0.17–0.49 wt.% NiO. Spinels are characterized by low Cr# values of 8.9–14.6 and low Mg# values of 66.2–73.1, thus plotting near the lower end of the Mid-Atlantic Ridge abyssal peridotite field of the Cr#–Mg# diagram (Figure 6b; Dick, 1989; Choi et al., 2008). In addition, spinels have markedly low TiO_2 contents, commonly less than 0.1 wt.%.

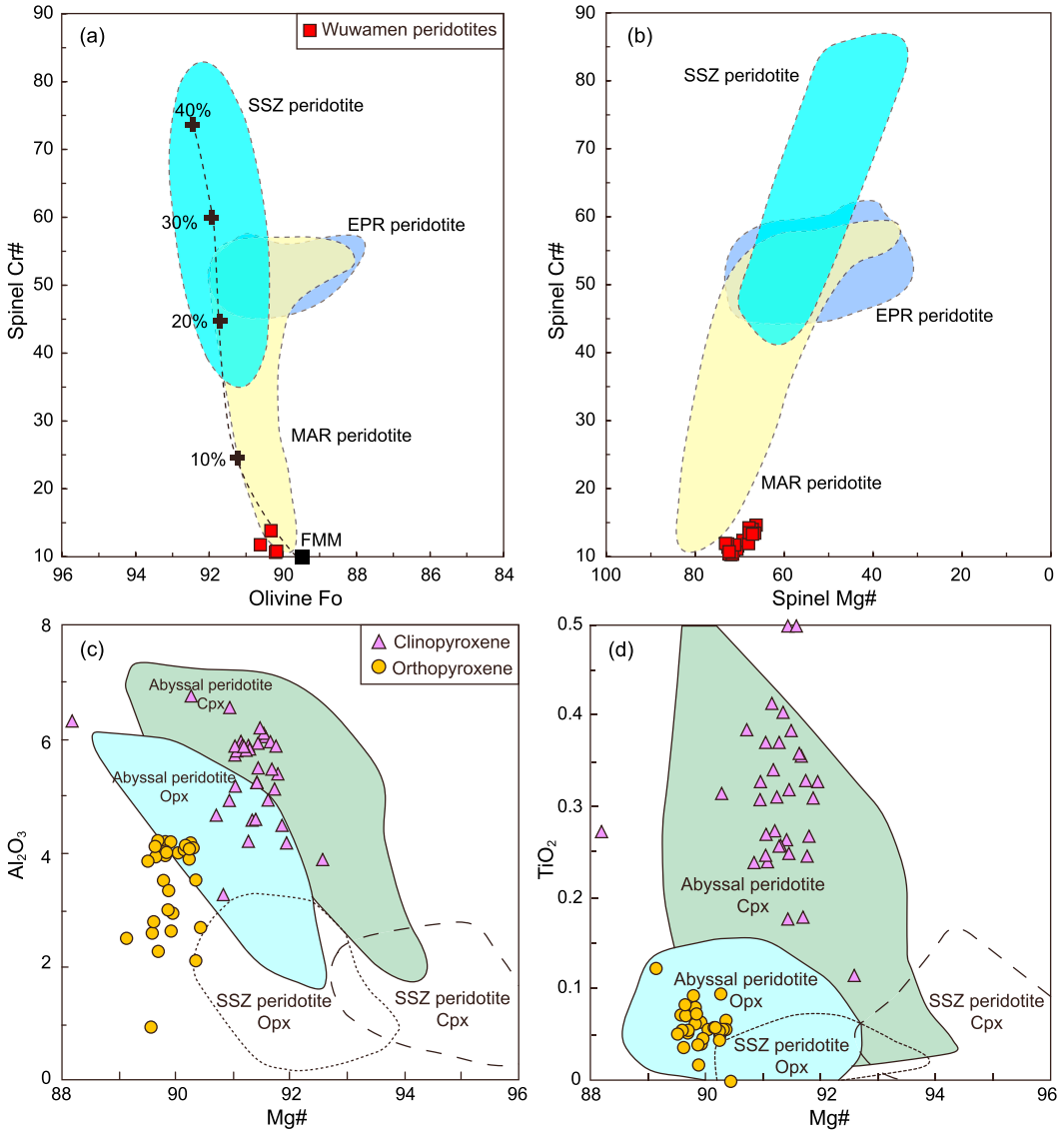

Figure 6. (a) Spinel Cr# versus olivine Fo and (b) spinel Mg# for the mantle peridotites in the Wuwamen ophiolitic mélange. Fields of abyssal peridotites from Mid-Atlantic Ridge (MAR; Dick, 1989), East Pacific Rise (EPR; Allan & Dick, 1996; Dick & Natland, 1996; Edwards & Malpas, 1996), and suprasubduction zone peridotites (SSZ; Parkinson & Pearce, 1998; Pearce et al., 2000) are shown for comparison. FMM = fertile MORB mantle. (c and d) Pyroxene Al_2O_3 and TiO_2 versus Mg# plots. Fields of orthopyroxene (Opx) and clinopyroxene (Cpx) of the abyssal peridotites and the SSZ peridotites are after Choi et al. (2008), and references therein.

Orthopyroxenes are mainly enstatites ($En_{87.3–89.5}Wo_{0.3–2.1}$) with Mg# values of 89.1–90.4 similar to those of olivines (Table S1 and Figure 6). Most orthopyroxenes show relatively scattered contents of Al_2O_3 (2.09–4.20 wt.%), Cr_2O_3 (0.12–0.72 wt.%), and TiO_2 (0–0.12 wt.%) and thus plot close or within the field of abyssal peridotites in the Al_2O_3–Mg# and TiO_2–Mg# diagrams (Figure 6). Clinopyroxenes are mainly diopsides ($En_{42.9–55.2}Wo_{36.3–46.9}$) with Mg# values of 90.3–92.6. They further exhibit high Al_2O_3 (3.24–6.73 wt.%), Cr_2O_3 (0.39–0.95 wt.%), and TiO_2 (0.12–0.50 wt.%) contents and also plot into the field of abyssal peridotites (Figure 6). In addition, ten clinopyroxene grains that were analyzed for trace elements display depleted rare earth element (REE) patterns with variably depleted light rare earth elements (LREEs) relative to flat heavy rare earth elements (HREEs; Figure S2). They further show notable Sr–Zr negative anomalies and relatively weak Ti negative anomalies.

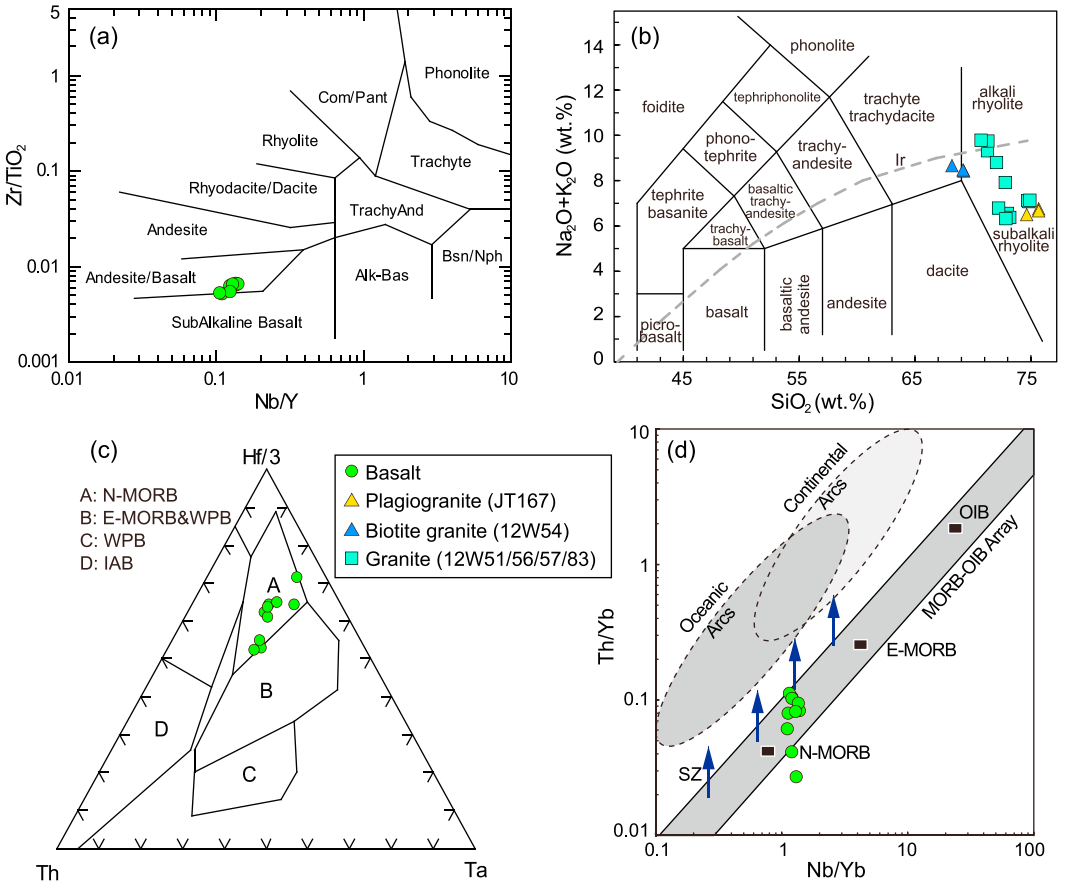

Figure 7. Geochemical classification and discrimination diagrams for the igneous rocks from the Wuwamen ophiolitic mélange. (a) Zr/TiO_2–Nb/Y plot (Winchester & Floyd, 1977). (b) TAS diagram (Le Bas et al., 1986). (c) Hf/3–Th–Ta diagram (Wood, 1980). (d) Th/Yb versus Nb/Yb diagram (Pearce, 2014).

4.2. Geochemistry of the Basalts

Whole-rock major and trace element and Sr–Nd isotopic compositions of basalts from the Wuwamen ophiolite are listed in Tables S2 and S3. The basalts were generally subject to pervasive alteration and deformation, and some were metamorphosed under greenschist- to amphibolite-facies conditions (Figure S1). Locally, pillow structures are well preserved (Figure 4). Ten samples have loss-on-ignition (LOI) contents of 1.16–8.45 wt.%, consistent with variable alteration overprints. They show a narrow range of SiO_2 (44.72–54.00 wt.%), TiO_2 (0.84–1.44 wt.%), and MgO (5.13–8.18 wt.%) contents (Table S2). All basalts plot in the basalt field of the Nb/Y–Zr/Ti diagram (Figure 7a; Winchester & Floyd, 1977). They exhibit N-MORB-like REE patterns with a relative LREE depletion and flat HREEs ($[La/Yb]_N$ = 0.78–1.01) as well as N-MORB-like patterns on the primitive mantle-normalized trace element diagram (Figure 8). Furthermore, five basalt samples, which were analyzed for Sr–Nd isotopes, yielded a small range of initial $^{87}Sr/^{86}Sr$ ratios (0.70817 to 0.70881) and $\varepsilon_{Nd}(t)$ values (+4.91 to +7.98) when calculated using t = 443 Ma (Table S3).

4.3. Gabbro and Plagiogranite Stocks Crosscutting the Mantle Peridotites

A small gabbro stock (3 × 15 m) intruded the serpentinitized peridotite as displayed by the untectonized contact and the injection of small apophyses from the gabbro into the peridotite (Figure 4a). The gabbro underwent pervasive carbonatization with few clinopyroxene relics (Figure S1). Two samples (JT83A and JT83B; GPS: N42°37′41″, E86°15′40″) were collected for SIMS zircon U–Pb dating (Table S4). Zircon grains are very complex in the cathodoluminescence (CL) images: euhedral and prismatic grains generally show clear oscillatory zoning typical for magmatic zircon, while subrounded grains display irregular patchy or nebular zoning typical for metamorphic zircon (Figure 9; Corfu et al., 2003). Fifty-two grains from the two samples were

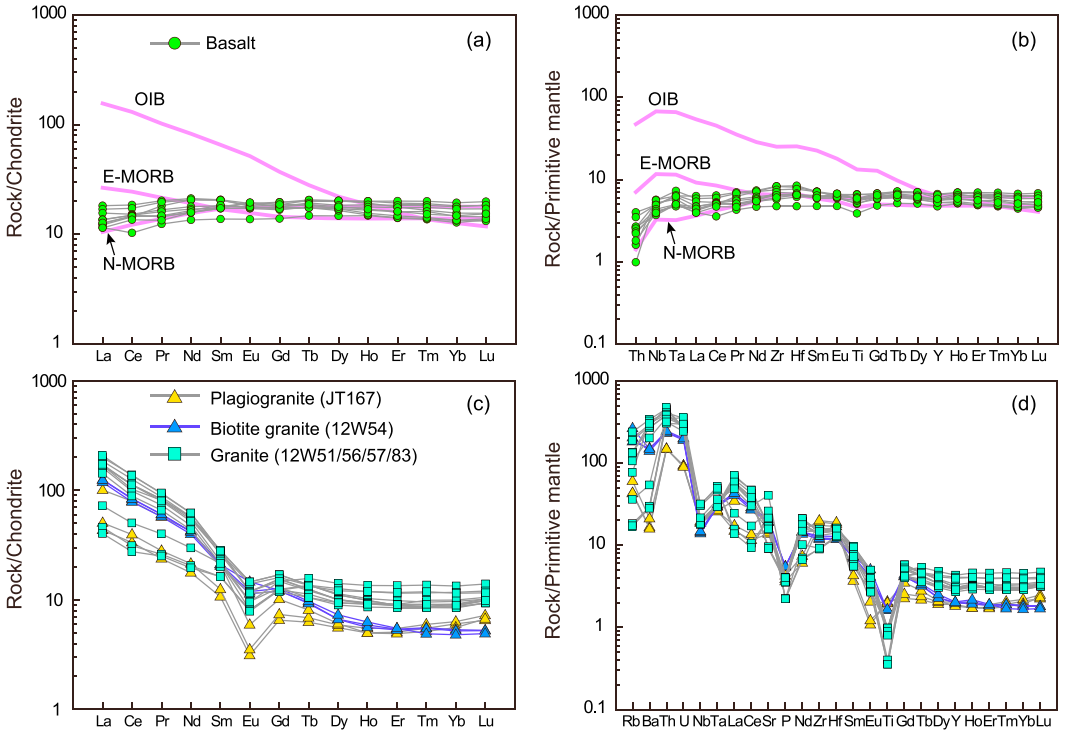

Figure 8. Chondrite-normalized REE patterns and primitive mantle-normalized multitrace element diagrams for the igneous rock units of the Wuwamen ophiolitic mélange. The normalized values of chondrite, primitive mantle, N-MORB, E-MORB, and OIB are from Sun and McDonough (1989).

analyzed, yielding scattered U–Pb ages between 2004 and 426 Ma with a 90–110% concordancy (except one outlier; Table S4). On the concordia diagram, 24 analyses with Precambrian ages of 2004–616 Ma, which display complex CL images including clear concentric and patchy zoning, were interpreted as xenocrysts. In contrast, the remaining 27 analyses with clear oscillatory zoning produced relatively uniform ages of 467–426 Ma with a mean age of 441.1 ± 4.2 Ma (MSWD = 2.6; Figure 9a).

In addition, a small plagiogranite stock (8 × 10 m) intruded the carbonated peridotites (Figure 4c) and consists mainly of fine-grained plagioclase and quartz (Figure S1). One sample (JT167; GPS: N42°37′36″, E86°16′20″) was chosen for LA-ICP-MS zircon U–Pb dating and Lu–Hf isotopic analyses (Tables S5 and S6). Zircon grains are generally euhedral and prismatic with clear concentric zoning in CL images, indicating a magmatic origin (Figure 9). Seventeen analyses on 17 grains yielded homogeneous $^{206}Pb/^{238}U$ ages ranging from 452 to 435 Ma and produced a concordia age of 442.8 ± 2.4 Ma (MSWD = 0.19; Figure 9b). However, they yielded highly heterogeneous initial $^{176}Hf/^{177}Hf$ ratios of 0.282104–0.282739 and $\varepsilon_{Hf}(t)$ values from −13.9 to +8.6, with corresponding two-stage model ages (T_{DM2}) ranging between 2303 and 879 Ma (Table S6).

Furthermore, three samples (JT167–1, −2, −3) from the plagiogranite stock were taken for whole-rock geochemical analyses (Table S2). The samples are granites (Figure 7) as indicated by high SiO_2 contents (74.7–75.4 wt.%). They are further characterized by high Na_2O (5.48–6.22 wt.%) and very low K_2O (0.70–1.02 wt.%) contents (Table S2), consistent with plagioclase as the main feldspar phase. In addition, they display LREE-enriched patterns, as shown by highly fractionated LREE, flat to concave HREE patterns and notable Eu negative anomalies (Eu/Eu* = 0.37–0.40; Figure 8c). On the primitive mantle normalized spiderdiagram (Figure 8d), they exhibit enrichments of large-ion lithophile elements (LILEs: Rb, Ba, Th, U) relative to depletions of compatible elements and weak negative Nb, Ta, and Ti anomalies.

4.4. Matrix and Intruding Granite Dike

One sericite-quartz schist sample (JT86; GPS: N42°37′10″, E86°16′11″) from the mélange matrix (Figure 4) was collected for LA-ICP-MS detrital zircon U–Pb dating (Table S6). The sample is mainly composed of sericite,

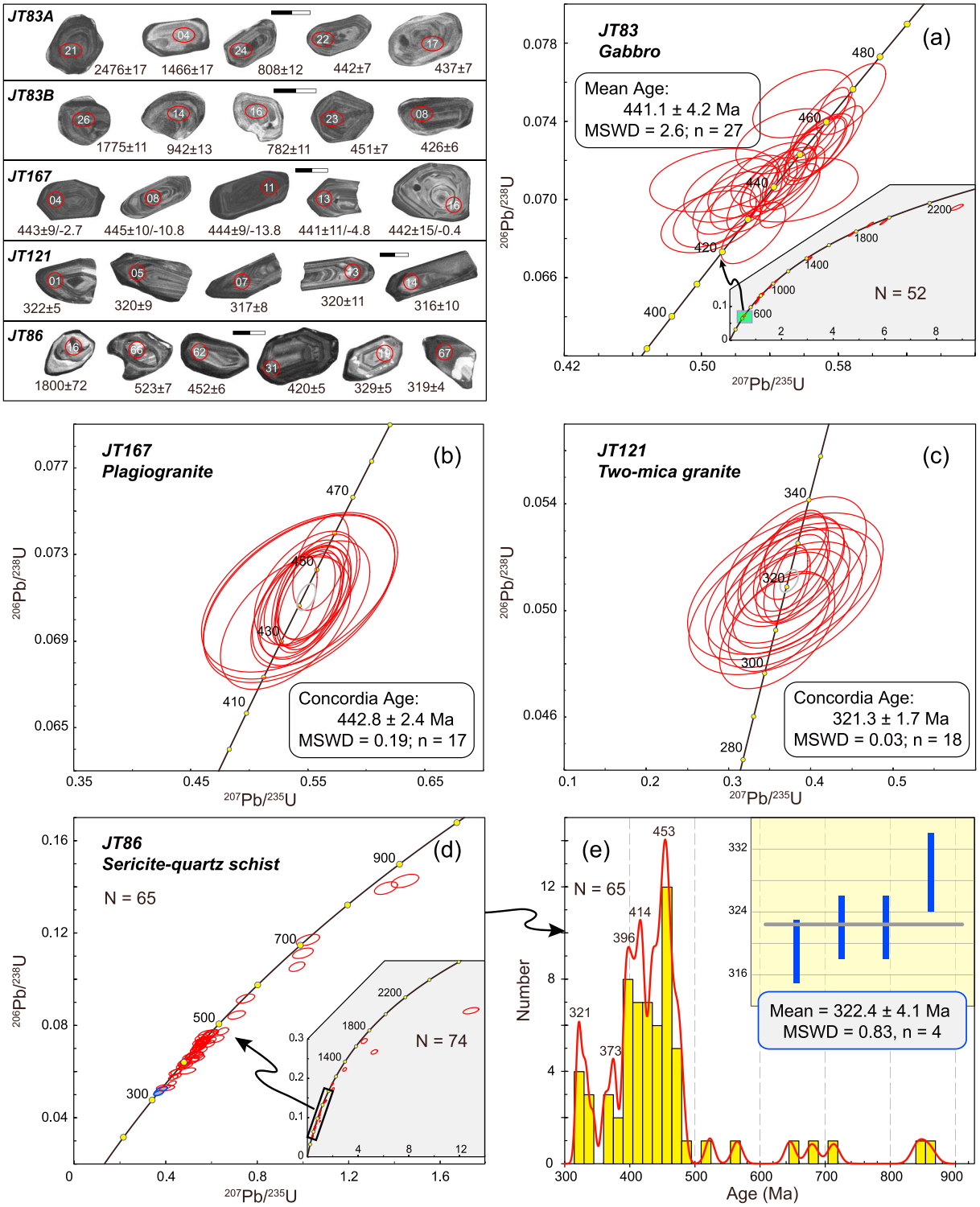

Figure 9. Zircon U–Pb concordia diagrams for different lithologies in the Wuwamen ophiolitic mélange. (a) Sample JT83 from the gabbro stock intruding the mantle peridotites. (b) Sample JT167 from the plagiogranite stock crosscutting the mantle peridotites. (c) Sample JT121 from the two-mica granite dike intruding the mélange matrix. (d and e) Detrital zircon U–Pb concordia and relative probability diagrams for sample JT86 from the matrix. Note that representative CL images are presented to show zircon internal textures. The apparent ages are indicated, in which $\varepsilon_{Hf}(t)$ values are also marked for sample JT167. The scale bars are 50 μm in length.

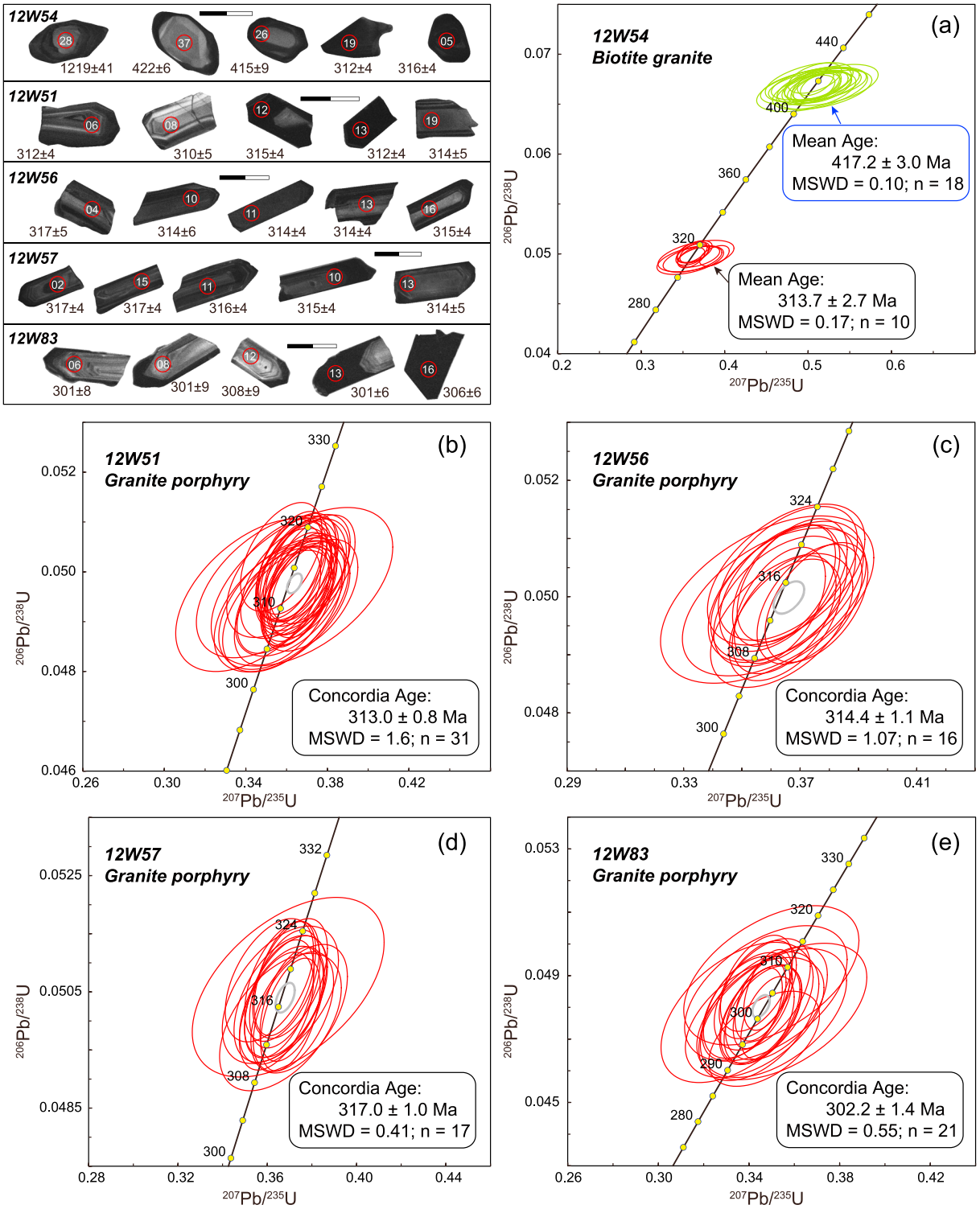

Figure 10. Zircon U–Pb concordia diagrams for five granite dikes and/or sills in the Precambrian fragments of the Yangjuan area, northwest of the Wuwamen ophiolitic mélange. Selected CL images are presented to show zircon internal textures and their apparent ages. The scale bars are 100 μm in length.

quartz, and minor plagioclase porphyroclasts with a south dipping foliation (Figure S1). Most zircon grains exhibit euhedral, prismatic morphologies and clear oscillatory zoning patterns, typical of a magmatic origin (Figure 9). Few grains display irregular or subrounded shapes and complex zoning patterns,

including sector and homogeneous zonings, with rare anhedral inherited core domains (Figure 9). Sixty-seven analyses on 74 zircon grains yielded near-concordant or concordant ages within a concordancy of 95–110% (Table S6 and Figure 9d). The U–Pb ages mainly range in a continuous spectrum between 481 and 319 Ma, while a few older ages of 1800–565 Ma are displayed by irregular or subrounded grains (Figure 9e). Notably, the four youngest zircon grains produced a weighted mean age of 322.4 ± 4.1 Ma (MSWD = 0.83; Figure 9e).

Toward the northwest of the Wuwamen ophiolite mélange, a granite dike intruded the mylonitized biotite-quartz schist matrix (Figures 3 and 4). The granite dike shows a typical porphyritic texture defined by K-feldspar phenocrysts in a groundmass of mica and quartz (Figure S1). Notably, the two-mica granite dike was subject to intensive mylonitization with a south dipping foliation marked by mica aggregates, similar to the foliation of the matrix. One sample (JT121; GPS: N42°38′19″, E86°12′30″) from the granite dike was collected for LA-ICP-MS zircon U–Pb dating (Table S5). Zircon grains are euhedral and long prismatic with clear concentric zoning, typifying magmatic zircon (Figure 9). Eighteen analyses yielded $^{206}Pb/^{238}U$ ages from 329 to 310 Ma and gave a concordia age of 321.3 ± 1.7 Ma (MSWD = 0.03; Figure 9c).

4.5. Granites in the Precambrian Fragments

In the northwest of the Wuwamen ophiolitic mélange, several granite dikes and/or sills intruded a Precambrian basement fragment (Figures 3 and 5), which is mainly composed of ~2.5 Ga amphibolite-facies volcano-sedimentary assemblages (Wang, Gao, et al., 2017). These variably sized dikes generally crosscut the foliation of the host rocks. All dikes show typical porphyritic textures with phenocrysts of feldspar and quartz in a fine-grained groundmass. In addition, the dikes are variably overprinted by ductile shearing, as indicated by subgrain formation of phenocrysts, undulatory quartz, and oriented mica flakes (Figure S3). Five samples (12W54, 12W51, 12W56, 12W57, 12W83) were taken for LA-ICP-MS zircon U–Pb dating (Table S5). Zircon grains generally have euhedral and long prismatic morphologies while two contrasting internal textures are displayed in the CL images. The CL-bright grains show clear oscillatory zoning typical of a magmatic origin, while the CL-dark grains occur as single crystals or overgrowths similar to those of hydrothermal zircon (Corfu et al., 2003; Hoskin, 2005). A total of 122 spots were analyzed on 122 zircon grains. The analyses positioned on the homogeneous CL-dark regions generally have higher contents of Th and U than those on the oscillatory zoned domains (Table S5). With respect to 12W54 (GPS: N42°40′30″, E86°04′03″), seven spots on the core domains yielded older ages of 2402–597 Ma and were accordingly interpreted as xenocrysts from the wall rocks. Except two discordant analyses, the remaining 28 spots define two distinct age clusters (Figure 10a): an upper one with a mean age of 417.2 ± 3.0 Ma (MSWD = 0.10; n = 18) for the oscillatory zoned domains and a lower one with a mean age of 313.7 ± 2.7 Ma (MSWD = 0.17; n = 10) for the unzoned CL-dark regions. In contrast, analyses on the oscillatory zoned and unzoned CL-dark zircon domains of the remaining four samples (12W51, 12W56, 12W57, 12W83) yielded—within errors—indistinguishable concordia U–Pb ages of 313.0 ± 0.8 Ma (MSWD = 1.6; n = 31), 314.4 ± 1.1 Ma (MSWD = 1.07; n = 16), 317.0 ± 1.0 Ma (MSWD = 1.0; n = 17), and 302.2 ± 1.4 Ma (MSWD = 0.55; n = 21), respectively (Figures 10b–10e).

Fifteen samples were chosen for whole-rock geochemical analyses (Table S2). The samples have relatively high SiO_2 contents of 68.23–74.96 wt.% and thus plot in the trachydacite and rhyolite fields of the TAS diagram (Figure 7b). They further display high contents of Al_2O_3 (13.9–15.4 wt.%) and $Na_2O + K_2O$ (6.32–9.78 wt.%; Table S2). In addition, these samples show LREE-enriched patterns with weak to moderate Eu negative anomalies (Eu/Eu^* = 0.50–0.91; Figure 8c). On the primitive mantle-normalized trace element diagram, the samples show variable LILE enrichments relative to the compatible elements as well as weak to prominent Nb, Ta, P, and Ti negative anomalies (Figure 8d).

5. Discussion

5.1. Nature, Formation, and Emplacement of the Wuwamen Ophiolite

Ophiolites have been interpreted to form in various tectonic settings, including mid-ocean ridge (MOR) and suprasubduction zone (SSZ) settings (e.g., Dilek & Furnes, 2011, 2014; Pearce, 2014). Both the mineral chemistry of mantle peridotites and the geochemical composition of erupted lavas were employed to fingerprint the precise setting of ophiolites (e.g., Arai, 1994; Choi et al., 2008; Dilek & Furnes, 2011; Miyashiro, 1973;

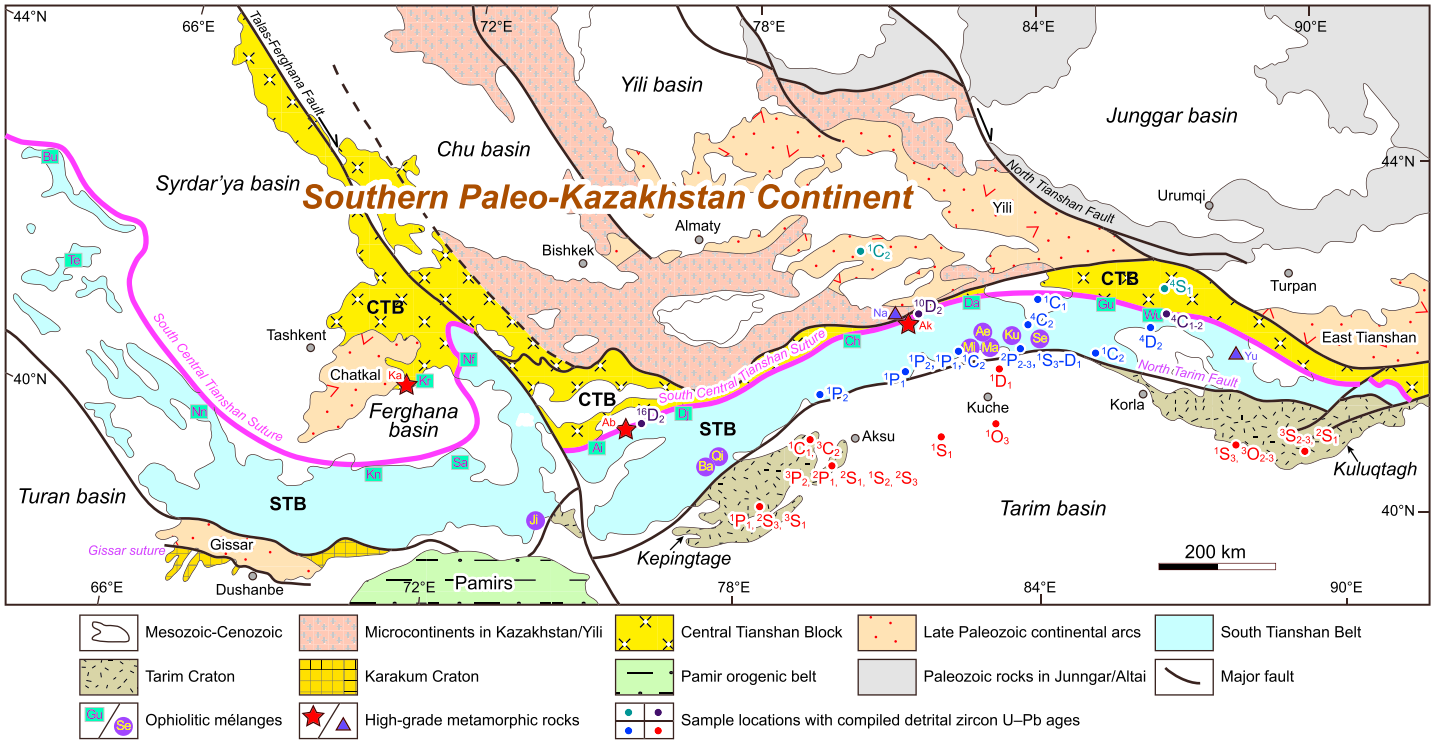

Figure 11. Tectonic sketch map of the southwestern CAOB (modified after Alexeiev et al., 2015, 2016; Gao et al., 2015) showing the ophiolitic mélanges, high-grade metamorphic rocks, and samples with compiled detrital zircon U–Pb ages in the South Tianshan and adjacent areas. The northern ophiolitic belt (marked by bright green rectangles) along the South Central Tianshan Suture Zone is interpreted to represent relics of the South Tianshan Ocean, from east to west including the Wuwamen (Wu), Guluogou (Gu), Dalubayi (Da), Changawuzi (Ch), Djanydjer (Dj), Aigyrbulak (Ai), North Ferghana (Nf), Karaterek (Kr), Sartale (Sa), Kan (Kn), North Nuratau (Nn), Teskuduk (Te), and Bukantau (Bu) ophiolites. The southern belt (denoted by purple circles) along the North Tarim Fault comprises the Serikeyayilake (Se), Kulehu (Ku), Aertengkesi (Ae), Madaleke (Ma), Misibulake (Mi), Qiqijianake (Qi), Baleigong (Ba), and Jigen (Ji) ophiolites, which are thought to represent relics of a back-arc basin rifted off the northern Tarim Craton during the mid-Paleozoic southward subduction of the South Tianshan Ocean. High-grade metamorphic rocks include several HP/LT belts [Akyazi (Ak), Atbashi (Ab), and Kassan (Ka)] and high-temperature metamorphic complexes [Yushugou HP/HT granulite (Yu) and Nalati migmatite complex (Na)]. (Meta)sedimentary rock samples with compiled detrital zircon age data are indicated by small circles in different colors with sample number labels as superscripts followed by their approximate depositional ages (see data sources in Table S9).

Pearce, 2008, 2014; Wang et al., 2015). In this study, the mantle peridotites of the Wuwamen ophiolite show extremely low spinel Cr# values (8.9–14.6) and all analyses plot near the lower end of the field defined by abyssal peridotites from the Mid-Atlantic Ridge (Figure 6). Generally, SSZ peridotites have higher spinel Cr# values, which are thought to be a result of higher degrees of partial melting due to slab-derived fluid fluxing in subduction-related settings (Choi et al., 2008; Parkinson & Pearce, 1998; Pearce et al., 2000). In addition, pyroxenes from the mantle peridotites have relatively low MgO, high Al_2O_3, and TiO_2 contents compared to those of SSZ peridotites and thus plot within or close to the MOR abyssal peridotite fields (Figure 6). Furthermore, clinopyroxenes display LREE-depleted patterns corresponding to an estimated 5% fractional melting of a depleted MORB mantle (DMM) source (Figure S2; Liu, Zhang, et al., 2016; Workman & Hart, 2005), which is consistent with the low spinel Cr# values indicative of a very low degree (less than 5%) melting (Hellebrand et al., 2001). The clinopyroxenes have remarkably high Ti and HREE contents and plot in the fields of abyssal peridotites along the dry melting trends (Figure S2), suggesting an origin associated with dry melting of a DMM source rather than hydrous melting above a subduction zone (Bizimis et al., 2000). Therefore, it seems more likely that the Wuwamen ophiolite originated in a mid-ocean ridge setting.

Since ophiolites typically undergo pervasive alteration or metamorphism during their transport from the ridge through the subduction zone to the orogenic belt, immobile elements for fingerprinting of basalts should be carefully chosen (Cann, 1970; Pearce, 2008, 2014). Thus, binary diagrams of LOI versus major and trace elements for the basalts were employed to assess the overall element mobility (Figure S4). Our results suggest that TiO_2, Al_2O_3, HFSEs (Th, U, Nb, Ta, Zr, Hf), and REEs behaved relatively immobile, while SiO_2, MgO, and CaO may have been variably enriched and K_2O, Cs, Rb, Ba, and Sr variably depleted during

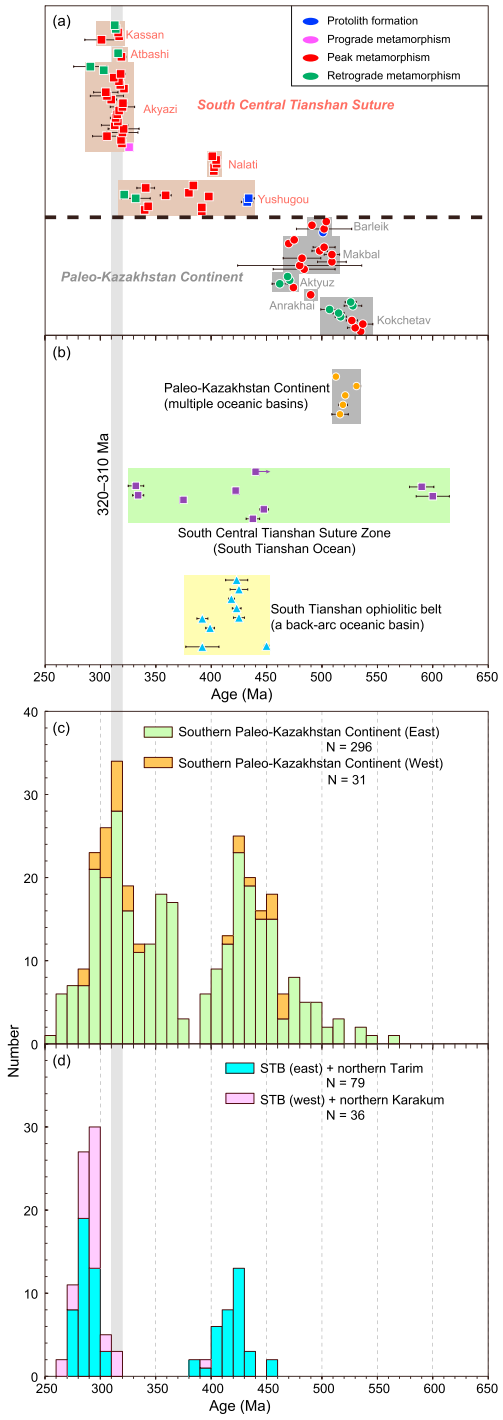

Figure 12. (a) Metamorphic age compilation of high-grade metamorphic rocks in the Paleo-Kazakhstan Continent and the South Central Tianshan Suture Zone (see data sources in Table S11). (b) Compilation of formation ages for ophiolitic mélanges in the Paleo-Kazakhstan Continent, the South Central Tianshan Suture Zone, and the South Tianshan ophiolitic belt (see data sources in Table S10). (c and d) Histograms of compiled crystallization ages of igneous rocks in the southern Paleo-Kazakhstan Continent, the South Tianshan Belt (STB), the northern Tarim, and the northern Karakum (see Table S8 for data sources). Note that the igneous rocks in the southern Paleo-Kazakhstan Continent and STB are divided into eastern and western groups concerning their positions with regard to the Talas-Ferghana strike-slip fault.

alteration and/or metamorphism. As a result, discrimination diagrams employing rather immobile elements were selected for geochemical fingerprinting of the ophiolitic basalts. In the Hf–Th–Ta diagram all basalt analyses fall into the N-MORB field (Figure 7c). In addition, in the Nb/Yb versus Th/Yb diagram, all basalts plot close to typical N-MORB compositions without a prominent shift to higher Th/Yb ratios, thereby indicating a negligible subduction-derived contribution to their mantle source (Figure 7d; Pearce, 2014). This is consistent with their N-MORB-similar REE and multitrace element patterns, as well as the highly positive $\varepsilon_{Nd}(t)$ values (+4.91 to +7.98) that are similar to that of depleted mantle (+8.6; Goldstein et al., 1984). Consequently, all evidence suggests that the N-MORB-type basalts from the Wuwamen ophiolite were derived from a depleted mantle source. In summary, both the mineral chemistry of the mantle peridotites and the geochemical signature of the basalts suggest that the Wuwamen ophiolite is a MOR-type ophiolite formed in a mid-ocean ridge setting.

Due to the absence of gabbros or sheeted dikes the formation age of the Wuwamen ophiolite is not precisely known. An OIB-like andesite with arc signatures, which was interpreted as an ophiolitic component, revealed a zircon U–Pb age of 309 ± 4 Ma (Wang, Zhai, et al., 2017). However, its highly negative $\varepsilon_{Nd}(t)$ value (−11.6) is inconsistent with a mid-ocean ridge formation of the Wuwamen ophiolite. The here dated gabbro and plagiogranite stocks that intruded the mantle peridotites provide a minimum age for the ophiolite formation and emplacement. The mean age of 441.1 ± 4.2 Ma for magmatic zircon grains from the gabbro stock represents its intrusive age. Notably, the large population of 2004–616 Ma zircon grains with complex morphologies and internal textures indicate a xenocrystic origin from the CTB basement rocks during the gabbro intrusion. In addition, the 442.8 ± 2.4 Ma concordia age of the plagiogranite stock is interpreted as the crystallization age. The plagiogranites exhibit arc-type geochemical signatures, such as LREE and LILE enrichments relative to HREE and HFSE as well as negative Nb, Ta, and Ti anomalies. In conjunction with the highly scattered zircon $\varepsilon_{Hf}(t)$ values (−13.9 to +8.6), the plagiogranite stock is interpreted to have formed in a continental margin setting. Considering the temporal and spatial correlations with the ~450–420 Ma arc-related gabbroic and dioritic plutons in the vicinity (Zhong et al., 2015), the gabbro and plagiogranite stocks are thought to have formed in a continental arc setting at ~440 Ma. These results suggest that the mélange gabbro and plagiogranite do not represent ophiolite elements and that the Wuwamen ophiolite was formed and got emplaced on the continental margin prior to the intrusion of the stocks, i.e., before ~440 Ma.

5.2. STB: An Accretionary Complex or a Continental Arc?

Due to the presence of various rock types of different origins the nature and tectonic affinity of the STB is highly debated, which hampers the reconstruction of the South Tianshan Orogen. In early models, the STB was regarded as a north facing passive margin connected to the Tarim Craton during Paleozoic northward oceanic subduction (e.g., Gao et al., 1998; Han et al., 2011; Windley et al., 1990). The southern ophiolitic belt was interpreted as thrust klippes derived from the northern belt (Figure 11), and thus representing relics of a single

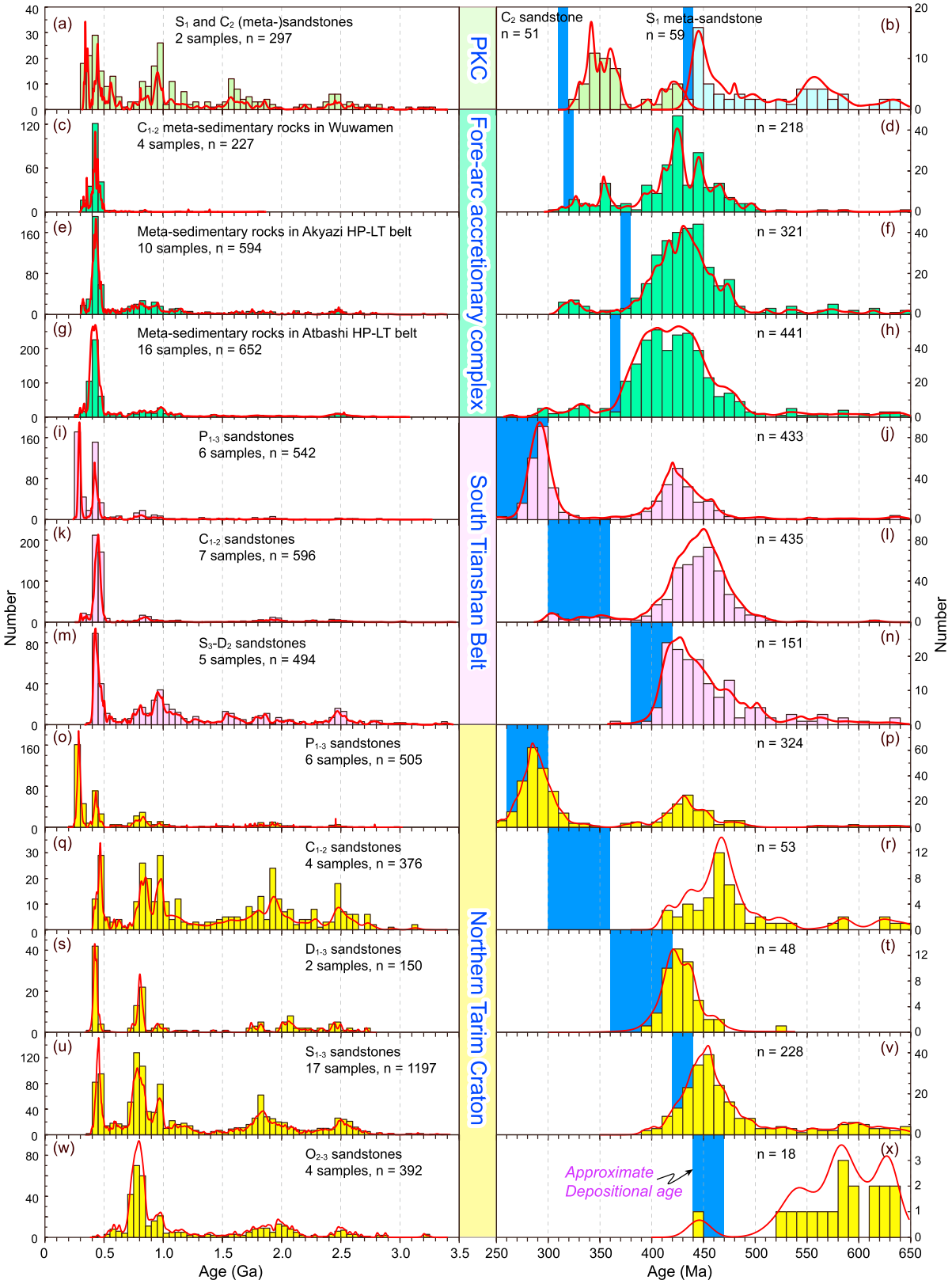

Figure 13. Histograms and probability curves for compiled detrital zircon U–Pb ages of (meta)sedimentary rocks with different depositional ages (indicated by dark blue bars) from the southern Paleo-Kazakhstan Continent (PKC), the fore-arc accretionary complex in the South Central Tianshan Suture Zone, the South Tianshan Belt, and the northern Tarim Craton. The locations of the complied samples are denoted in Figure 11. Data sources are presented in Table S9.

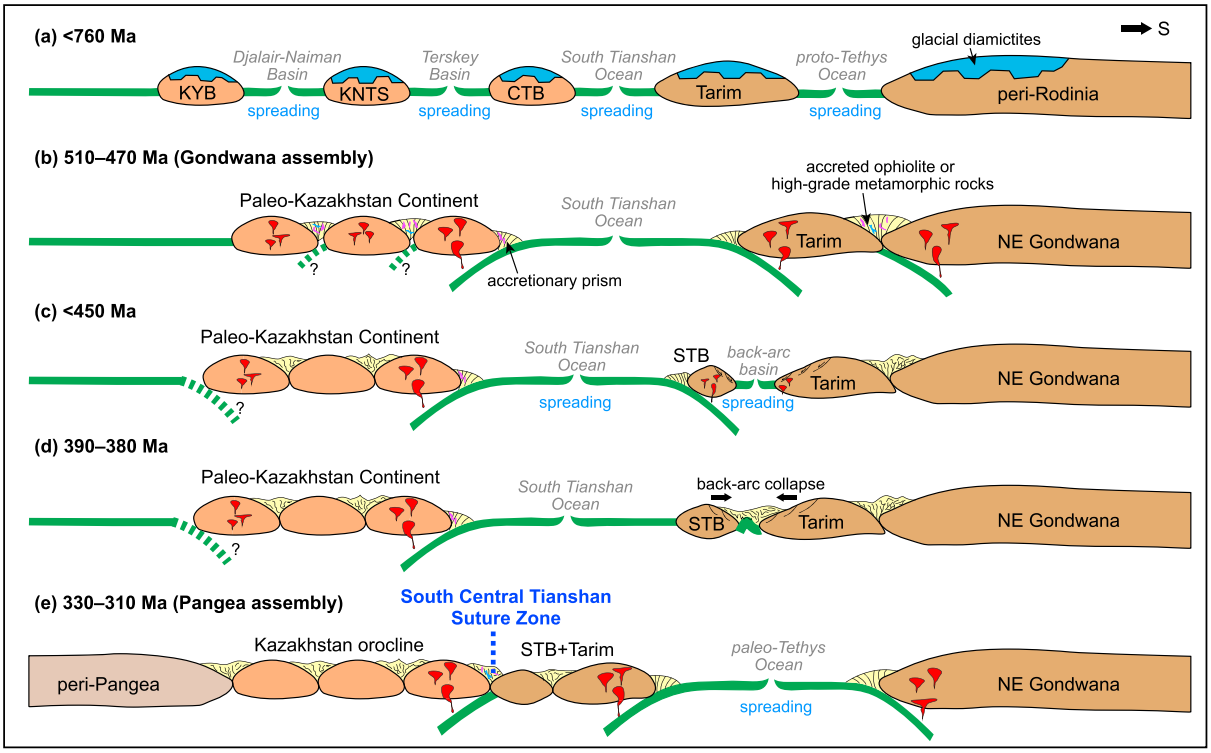

Figure 14. Cartoon showing the tectonic evolution of the microcontinents in the southwestern CAOB and adjacent areas with links to Gondwana and Pangea during late Cambrian to late Carboniferous times. KYB: Kazakhstan–Yili Block, KNTS: Kyrgyz North Tianshan, CTB: Central Tianshan Block, STB: South Tianshan Belt.

ocean basin (i.e., the South Tianshan Ocean; Gao et al., 1998; Han et al., 2011; Han & Zhao, 2017). However, 450–380 Ma arc-type granitoids in both the STB and northern Tarim Craton indicate the development of an active continental arc during this period (e.g., Ge, Zhu, Wu, et al., 2012; Ge, Zhu, Wilde, He, et al., 2014; Huang et al., 2013; Lin et al., 2013; Zhao et al., 2015). In addition, some authors suggested that the STB was connected to the Chinese Central Tianshan as an active continental arc above the south directed subducting Central Tianshan or Paleo-Tianshan Ocean (Lin et al., 2009; Charvet et al., 2011; Wang et al., 2011; Wang, Zhai, et al., 2017). However, a compilation of age data of Paleozoic igneous rocks shows that the Chinese Central Tianshan recorded continuous magmatism, at least between 500 and 250 Ma, in contrast to the STB and the northern Tarim Craton that are characterized by two discrete episodes, i.e., 450–380 and 310–260 Ma (Table S8 and Figure 12; Han et al., 2015; Han, Zhao, Sun, et al., 2016). Moreover, available detrital zircon age data from Paleozoic (meta)sedimentary rocks reveal that the STB and northern Tarim Craton share a similar age spectra with an absence of 390–310 Ma grains in contrast to the Chinese Central Tianshan (Table S9 and Figure 13; Huang et al., 2013; Han et al., 2015; Han, Zhao, Sun, et al., 2016). Considering these data, the STB is neither the western extension of the Chinese Central Tianshan nor a broad accretionary complex that accreted generally southward and oceanward during northward oceanic subduction (Xiao et al., 2013).

The southern ophiolitic belt of the STB yielded ages restricted between 450 and 390 Ma (Table S10 and Figure 12) and exhibits geochemical affinities to SSZ-type ophiolites, in contrast to the northern ophiolite complexes with MOR-type affinities (this study; Jiang et al., 2014; Long et al., 2006; Wang et al., 2011). Notably, significant fractions of inherited zircon grains with ages of 2750–794 Ma were identified in the ophiolitic members of the Kulehu and Baleigong ophiolites (Long et al., 2006; Wang et al., 2007), probably indicating that the oceanic basin was underlain by a Precambrian basement. The ~826–707 Ma granitic gneisses and early Paleozoic volcanic rocks to the north of the southern ophiolites (Alexeiev et al., 2015) may suggest the presence of a concealed Andean-type continental arc in the STB. However, $^{40}Ar/^{39}Ar$ plateau ages of 370–356 Ma, which were determined for micas from the mylonitic metapelites and for amphiboles from the amphibolites of the southern ophiolitic mélanges, were interpreted to represent the time frame

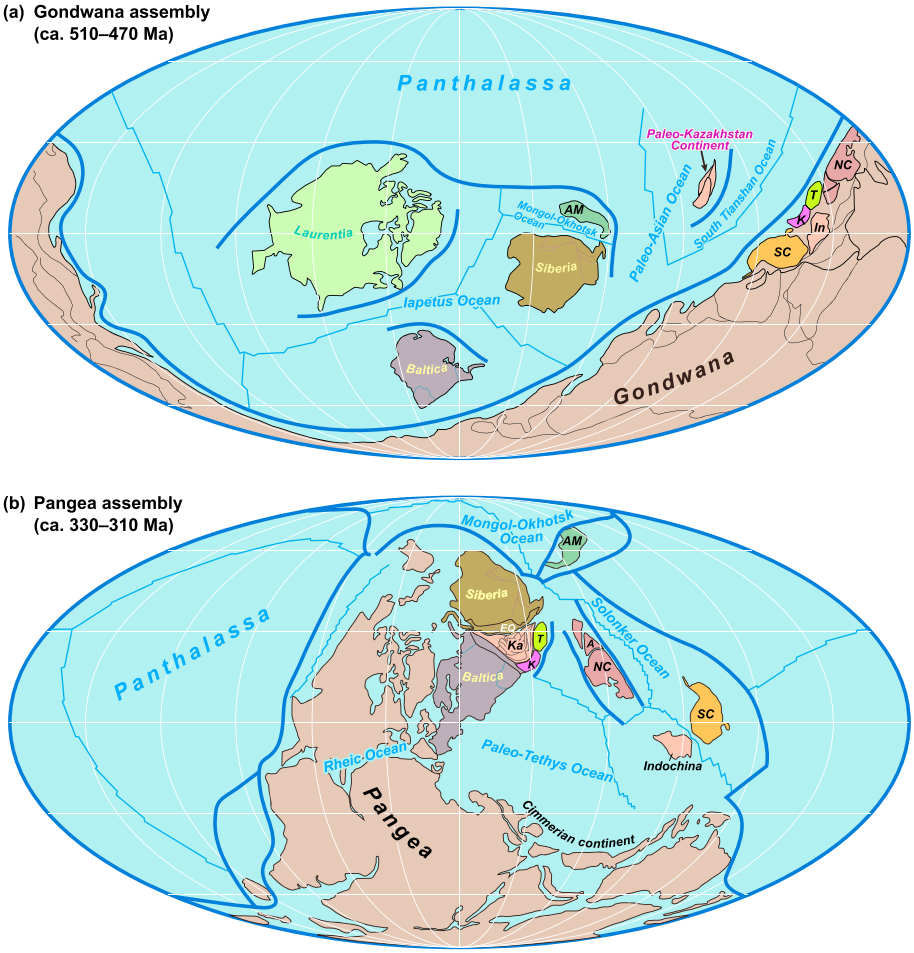

Figure 15. (a) Paleogeographic reconstruction during the Gondwana assembly at ~510–470 Ma (modified after Domeier, 2016; Han, Zhao, Cawood, et al., 2016; Metcalfe, 2013). Note that the Paleo-Kazakhstan Continent, which was formed during the assembly of Gondwana, is separated from the Tarim–Karakum cratons (i.e., NE Gondwana margin) by the South Tianshan Ocean. (b) Global map of Pangea paleogeography showing that the Paleo-Kazakhstan Continent and the Tarim–Karakum cratons were a part of Pangea at ~330–310 Ma (modified from Domeier & Torsvik, 2014). A = Alxa Block, AM = Amuria, EQ = Erqis, K = Karakum Craton, In = Indochina, Ka = Kazakhstan Orocline, NC = North China Craton, SC = South China Block, T = Tarim Craton.

of their tectonic emplacement (Han et al., 2011; Wang et al., 2011). This is evidenced by a regional angular unconformity between the mid-Devonian–late Carboniferous thick clastic–carbonate sequences and the Ordovician–early Devonian metamorphosed siliciclastic rocks and limestones (Han et al., 2015; Han, Zhao, Sun, et al., 2016; Wang et al., 2011). In addition, as shown by the detrital zircon age spectra of both the STB and the northern Tarim Craton (Figure 13), the Ordovician–early Devonian sedimentary rocks contain a large number of zircon ages close to their depositional ages, whereas the mid-Devonian–late Carboniferous sediments display an absence of zircon ages approximating the depositional ages, probably indicating transition from an active to a passive margin (Cawood et al., 2012). Thus, we propose that the STB constituted an Andean-type continental arc that connected to the northern Tarim Craton since at least ~500 Ma as indicated by the detrital zircon records (Figure 13). Subsequently, the STB rifted off as an isolated arc in response to the opening of a short-lived back-arc basin during 450–390 Ma and, finally, accreted to the northern Tarim Craton by transition into a north facing passive margin due to the closure of the back-arc basin (Figure 14).

5.3. Final Closure of the South Tianshan Ocean: How, When, and Where?

The interpretation of the STB as a short-lived continental arc, rather than a broad fore-arc accretionary complex, excludes that the final suturing of the southwestern CAOB occurred along a cryptic suture zone at the

base of the STB (cf. Xiao et al., 2013). Other authors argued that the final assembly of the CAOB occurred along the North Tianshan suture zone in the late Carboniferous subsequent to the collision of the KYB–CTB–STB and the northern Tarim Craton during late Devonian to early Carboniferous times (Charvet et al., 2011; Lin et al., 2009; Wang et al., 2008, 2010, 2011). The latter model is mainly based on the assumptions that (1) the regional angular unconformity during late Devonian–early Carboniferous times was related to the collision of the STB/CTB and the KYB, (2) eclogite-facies peak metamorphism as reflected by the (U)HP terranes took place at ~350–345 Ma, and (3) top-to-the-north thrusting of the (U)HP rocks over the KYB resulted from southward oceanic subduction. However, the origin of the regional angular unconformity is ambiguous since it could also have formed during ongoing subduction due to alternating contraction and extension on the upper plate, similar to the Andean orogenesis (e.g., Haschke et al., 2002). In addition, the eclogite-facies metamorphism of the (U)HP rocks occurred between ~326 and 310 Ma as revealed by numerous high-resolution isotopic methods (Figure 12 and Table S11; e.g., Su et al., 2010; Klemd et al., 2005, 2011; Li et al., 2016; Tan et al., 2017; Wang et al., 2018). Furthermore, top-to-the north thrusting of the (U)HP rocks may in fact represent the northern part of a positive flower structure in response to northward subduction beneath the KYB (Gao & Klemd, 2003), which is consistent with the development of regional high-temperature metamorphism to the north of the (U)HP rocks (Xia et al., 2014) as well as the subduction-related Yushugou HP granulites (Zhang et al., 2018; Zhang & Jin, 2016).

The results of this study indicate that the MOR-type Wuwamen ophiolite complex has been emplaced on the southern CTB prior to ~440 Ma. However, sericite-quartz schist of the mélange matrix comprises a major population of 481–319 Ma detrital zircon grains with the four youngest analyses producing a mean age of 322.4 ± 4.1 Ma. In combination with recently published data (see above), the mélange matrix age spectra differ from those of the STB and the northern Tarim Craton, but are similar to the continuous magmatic record of the CTB (Figures 12 and 13; Wang, Zhai, et al., 2017). Thus, we propose that the mélange matrix originated in a fore-arc accretionary complex by receiving detritus from the upper plate (i.e., the CTB) during ongoing northward subduction and was deposited at ~322 Ma as indicated by the youngest detrital zircon grains (Cawood et al., 2012; Wang, Zhai, et al., 2017). This is further supported by the 321.3 ± 1.7 Ma crosscutting two-mica granite dike, implying that the Wuwamen ophiolitic mélange formed at ~320 Ma.

Notably, the formation of the Wuwamen ophiolitic mélange is broadly coeval with the ~326–310 Ma peak metamorphism obtained for the (U)HP terranes along the SCTSZ, including Akyazi (China) and Atbashi (Kyrgyzstan) to the east and Kassan (Kyrgyzstan) to the west of the Talas–Ferghana Fault (Table S11 and Figures 11 and 12). The biotite granite sill in the Precambrian fragment of the Wuwamen ophiolitic mélange yielded ages of 417.2 ± 3.0 and 313.7 ± 2.7 Ma for oscillatory zoned magmatic zircon and unzoned CL-dark hydrothermal zircon, respectively. The former age is thought to represent the intrusive age of the sill during the northward oceanic subduction, while the latter is related to a hydrothermal event during collision. The other four granite dikes crosscutting the Precambrian fragment with ages of ~313–302 and 321 Ma two-mica granite dike intruding the mélange matrix are thus thought to have formed during the collision of the CTB and the united STB–Tarim Craton. When considering the ~330 Ma Guluogou ophiolite (Jiang et al., 2014) and the ~320 Ma Wuwamen ophiolitic mélange (this study), the SCTSZ (also called South Tianshan or Turkestan suture) formed coevally along its whole length at ~320 Ma (Mühlberg et al., 2016; cf. Loury et al., 2016) due to the final closure of the South Tianshan Ocean. This is consistent with the latest Carboniferous molasse-type conglomerate overlying the Atbashi (U)HP rocks (Hegner et al., 2010), the ~285 Ma postorogenic S-type leucogranite dike crosscutting the Akyazi (U)HP rocks (Gao et al., 2011), and the resumption of widespread magmatism in the STB and the northern Tarim Craton at ~310–270 Ma (Table S8 and Figure 12; e.g., Han & Zhao, 2017; Huang et al., 2014; Konopelko et al., 2007; Seltmann et al., 2011), all of which originated in a postcollisional setting. Therefore, these data reveal that the final suturing of the southwestern CAOB was achieved by northward subduction of the South Tianshan Ocean and subsequent collision of the CTB and the Karakum–Tarim cratons at ~320 Ma. Notably, recent studies suggest that a trench-arc–back-arc basin system developed in the northern Karakum during Carboniferous times (Konopelko et al., 2017; Worthington et al., 2017), which differs from the here suggested tectonic evolution that favors a transition of the northern Tarim Craton from a trench-arc–back-arc system to a passive margin at ~390–380 Ma.

5.4. Links With Gondwana and Pangea

The microcontinents (such as the CTB, KYB, KNTS) in the western CAOB and the Tarim Craton were interpreted to have been incorporated into the periphery of Rodinia through long-lived subduction-accretion processes, as evidenced by widespread late Mesoproterozoic to early Neoproterozoic magmatic rocks, and the ~830–790-Ma Aksu blueschists and HP granulites (Ge, Zhu, Wilde, He, et al., 2014; Ge et al., 2016; He et al., 2012; Kröner et al., 2012, 2013; Wang, Liu, et al., 2014). It was further suggested that these microcontinents and the Tarim Craton were detached from peri-Rodinia by back-arc rifting or plume-related breakup (e.g., Gao et al., 2015; Ge, Zhu, Wilde, He, et al., 2014; Ge, Zhu, Zheng, et al., 2012; Zhang, Li, et al., 2013), leading to the opening of multiple oceanic basins, such as the proto-Tethys Ocean between the Tarim Craton and northwest Australia (Zhang et al., 2009), and the South Tianshan, Terskey, and Djalair-Naiman oceanic basins as the southern branches of the Paleo-Asian Ocean (Figure 14; Gao et al., 2015; Ge, Zhu, Wilde, He, et al., 2014). This event is corroborated by the occurrences of extensive late Neoproterozoic (~760–600 Ma) ultramafic-mafic complexes, mafic dike swarms, alkaline granitoids, bimodal intrusions and volcanic rocks, late Neoproterozoic glacial diamictite interlayers, and Cambrian to early Ordovician phosphorous sequences in the western CAOB and the northern Tarim Craton (e.g., Ding et al., 2009; Ge, Zhu, Wilde, He, et al., 2014; Ge, Zhu, Zheng, et al., 2012; Han et al., 2015; Konopelko et al., 2014; Levashova et al., 2011; Wang, Shu, et al., 2014; Xu et al., 2009; Zhang, Li, et al., 2013; Zhang, Zou, et al., 2013). Thus, the opening of the South Tianshan Ocean may have started during the late Neoproterozoic, as indicated by the up to now oldest Dalubayi ophiolite with an age of ~600 Ma (Yang et al., 2005). Some authors proposed that the opening of the South Tianshan Ocean was initiated by back-arc rifting off the CTB from the northern Tarim Craton in the early Devonian (Han et al., 2015, Han, Zhao, Cawood, et al., 2016). However, this is inconsistent with the closure of the Terskey Ocean at ~470 Ma (Konopelko et al., 2012; Lomize et al., 1997; Qian et al., 2009) and the >440 Ma Wuwamen ophiolite (this study) as well as the ~448–422 Ma ophiolitic mélanges with early Ordovician to early Silurian fossils in the Kyrgyz South Tianshan (Table S10 and Figure 12; Alexeiev et al., 2016; Biske & Seltmann, 2010; Dolgopolova et al., 2017; Wang et al., 2016). In addition, Safonova et al. (2016) reported late Silurian to early Carboniferous elements consistent with an ocean plate stratigraphy in the Kyrgyz South Tianshan and thus suggested that the South Tianshan Ocean was a relatively large oceanic realm during this period.

The Tarim Craton to the south of the western CAOB was interpreted to have accreted to East Gondwana through collision with northern Australia and the closure of the proto-Tethys Ocean, as evidenced by 510–470 Ma (U)HP metamorphic events in the southern Altyn Tagh area (Han, Zhao, Cawood, et al., 2016; Zhang et al., 2014). Similar to the Tarim Craton, the Karakum Craton was thought to have been integrated in East Gondwana, and both cratons were interpreted as part of the Hunic composite terrane (Volkova & Budanov, 1999; von Raumer et al., 2003). At the same time, several microcontinents (such as the CTB, KNTS, KYB) in the western CAOB accreted to the Paleo-Kazakhstan Continent due to the closure of the Djalair-Naiman and Terskey oceanic basins (Figure 14; Wilhem et al., 2012; Windley et al., 2007), as evidenced by the ~530–470 Ma peak metamorphism of the (U)HP metamorphic terranes, including the Kokchetav, Anrakhai, Aktyuz, Markbal, and Barleik terranes (Table S11 and Figure 12; e.g., Klemd et al., 2014; Konopelko et al., 2012; Liu, Han, et al., 2016; Meyer et al., 2014; Rojas-Agramonte et al., 2013). However, no firm evidence exists that the South Tianshan Ocean between the Paleo-Kazakhstan Continent and the Karakum–Tarim cratons was already closed during the final assembly of Gondwana. Instead, the results of the present study suggest that the microcontinents in the western CAOB were not incorporated into Gondwana during this period but were rather separated from this supercontinent by the South Tianshan Ocean as a major barrier (Figure 15a).

Subsequently, the Paleo-Kazakhstan Continent was surrounded by the Ob-Zaisan, Uralian, Junggar, and South Tianshan oceans, and continuous subduction-accretion led to the addition of various terranes to the Paleo-Kazakhstan Continent, including the Aktau–Junggar Block, the Boschekul–Chingiz arc, the Baydulet–Akbastau arc, the Devonian Volcanic Belt, and the Balkhash–Yili arc (e.g., Li et al., 2018; Wilhem et al., 2012; Windley et al., 2007; Xiao et al., 2010, 2015). During late Devonian to early Carboniferous, the Paleo-Kazakhstan Continent moved northward approaching the southern margin of Siberia and underwent oroclinal bending to form the incipient Kazakhstan Orocline (Bazhenov et al., 2003, 2012; Li et al., 2018; Xiao et al., 2010, 2015). Meanwhile, continental blocks such as the Karakum, Tarim, South China, North China, and Indochina blocks were detached from the NE margin of Gondwana and migrated northward due to the

opening of the Paleo-Tethys Ocean during early–middle Devonian times (Domeier & Torsvik, 2014; Han, Zhao, Cawood, et al., 2016; Metcalfe, 2013). Specifically, the Karakum–Tarim cratons moved across the South Tianshan Ocean and approached the southern limb of the Kazakhstan Orocline. The closure of the Ob-Zaisan Ocean was constrained to have occurred in the late Carboniferous, probably at ~320 Ma (Kuibida et al., 2016; Li et al., 2014, 2017), leading to the docking of the northern limb of the Kazakhstan Orocline to southern Siberia. The closure of the Uralian Ocean was also thought to have occurred at ~320 Ma, leading to the collision of the exterior of the Kazakhstan Orocline with Baltica (Loury et al., 2016; Puchkov, 1997). Similarly, the Junggar Ocean probably closed between 325 and 316 Ma, as indicated by the youngest ophiolite and the stitching granitic plutons (Han et al., 2010; Xu et al., 2006). As discussed above, the South Tianshan Ocean closed at ~320 Ma finally resulting in the collision of the southern limb of the Kazakhstan Orocline with the Karakum–Tarim cratons. Thus, it is concluded that the western CAOB and the Karakum–Tarim cratons assembled with Laurussia and Siberia at ~320 Ma, constituting the northern part of Pangea (Figure 15b; Domeier & Torsvik, 2014; Metcalfe, 2013). In this context, it should be noted that the almost simultaneous closure of the Rheic Ocean in the late Carboniferous resulted in the collision of Laurussia and Gondwana, constituting western Pangea in Central and SW Europe (Figure 15b; Kroner & Romer, 2010).

6. Conclusions

Field observations show that the Wuwamen ophiolitic mélange in the Chinese South Tianshan is structurally sandwiched between the Central Tianshan Block (CTB) to the north and the South Tianshan Belt (STB) to the south. It mainly consists of tectonic blocks of various origins, including ophiolitic components, Precambrian fragments, and marine sedimentary rocks and limestones/marbles set in a matrix of turbidites, all of which were overprinted by intensive deformation and variable metamorphism. Olivines, spinels and pyroxenes in the mantle peridotites from the Wuwamen ophiolite are compositionally similar to those of abyssal peridotites and the basalts display N-MORB-type geochemical affinities, suggesting that the Wuwamen ophiolite was formed in a mid-ocean ridge setting. The formation age of the ophiolite is constrained by zircon U–Pb ages of ~443–441 Ma of the Andean-type arc-related gabbro and plagiogranite stocks that intruded the mantle peridotites. This implies that the South Tianshan Ocean has existed since at least ~440 Ma with a possible northward subduction leading to the emplacement of the Wuwamen ophiolite on the southern margin of the CTB. In addition, sericite-quartz schist from the mélange matrix yielded detrital zircon ages comparable to those of igneous rocks in the CTB. Furthermore, the mélange matrix is crosscut by a two-mica granite dike with a zircon U–Pb age of ~321 Ma, thereby suggesting that the Wuwamen ophiolitic mélange originated in a fore-arc accretionary complex with its final formation at ~320 Ma.

Finally, a tentative tectonic model is proposed to account for the available data of the igneous rocks, the detrital zircon ages, the ophiolites, and the high-grade metamorphic rocks in the southwestern CAOB. Our model highlights that the South Tianshan Ocean was a broad ocean evolving from its opening by separation of the CTB from circum-Rodinia in the late Neoproterozoic to final closure by the collision of the southwestern CAOB and the Karakum–Tarim cratons at ~320 Ma. During the final assembly of Gondwana, the microcontinents in the western CAOB accreted to the Paleo-Kazakhstan Continent, while the Karakum–Tarim cratons were incorporated into the northeastern Gondwana margin with the intervening South Tianshan Ocean as a major barrier. Subsequently, the northward subduction of the South Tianshan Ocean beneath the CTB may have lasted to its final closure. By contrast, the southward subduction led to a short-lived trench–arc–back-arc system along the northern Tarim Craton, represented by the STB (isolated from the northern Tarim) with a back-arc basin opening, and subsequently the active continental margin converted into a passive margin due to the closure of the back-arc basin. At ~320 Ma, the South Tianshan Ocean was closed resulting in the final assembly of the Karakum–Tarim cratons and the western CAOB as well as their incorporation into Pangea.

Acknowledgments
This work was funded by the National Natural Science Foundation of China (41390445 and 41025008), China Geological Survey (DD20160345), and the China Postdoctoral Science Foundation (2016M600127), as well as the Sino-German (CSC-DAAD) Postdoc Scholarship Program to Xin-Shui Wang. We greatly appreciate the reviews by Paul R. Eizenhöfer and one anonymous reviewer that significantly improved the paper. Editor-in-Chief Michael Walter and Associate Editor John Lassiter are thanked for the comments and the efficient editorial handling. We further thank D. Zhang for undertaking the EMPA analyses and Q.L. Li, L. Su, and Y. H. Yang for the assistance with SIMS and LA-ICP-MS zircon U–Pb dating and Hf analyses. D.S. Xue, B.Y. Gao, and C.F. Li are thanked for their help with the whole-rock elemental and Sr–Nd analyses. Analytical methods and data supporting this paper are available in the supporting information.

References

Alekseev, D. V., Aristov, V. A., & Degtyarev, K. E. (2007). The age and tectonic setting of volcanic and cherty sequences in the ophiolite complex of the Atbashe Ridge (southern Tien Shan). *Doklady Earth Sciences*, *413*, 380–383.

Alexeiev, D. V., Biske, Y. S., Wang, B., Djenchuraeva, A. V., Getman, O. F., Aristov, V. A., et al. (2015). Tectono-stratigraphic framework and Palaeozoic evolution of the Chinese South Tianshan. *Geotectonics*, *49*, 93–122.

Alexeiev, D. V., Kröner, A., Hegner, E., Rojas-Agramonte, Y., Biske, Y. S., Wong, J., et al. (2016). Middle to late Ordovician arc system in the Kyrgyz Middle Tianshan: From arc-continent collision to subsequent evolution of a Palaeozoic continental margin. *Gondwana Research*, *39*, 261–291.

Alexeiev, D. V., Ryazantsev, A. V., Kröner, A., Tretyakov, A. A., Xia, X., & Liu, D. Y. (2011). Geochemical data and zircon ages for rocks in a high-pressure belt of Chu-Yili Mountains, southern Kazakhstan: Implications for the earliest stages of accretion in Kazakhstan and the Tianshan. *Journal of Asian Earth Sciences*, *42*, 805–820.

Allan, J. F., & Dick, H. J. B. (1996). Cr-rich spinel as a tracer for melt migration and melt-wall rock interaction in the mantle: Hess Deep, Leg 147, In: C. Mevel, K. M. Gillis, J. F. Allan, P. S. Meyer (Eds.), Proceedings of Ocean Drilling Program, Scientific Results (pp. 157–172).

Arai, S. (1994). Characterization of spinel peridotites by olivine-spinel compositional relationships: Review and interpretation. *Chemical Geology*, *113*, 191–204.

Bazhenov, M. L., Collins, A. Q., Degtyarev, K. E., Levashova, N. M., Mikolaichuk, A. V., Pavlov, V. E., & Van der Voo, R. (2003). Paleozoic northward drift of the North Tien Shan (Central Asia) as revealed by Ordovician and Carboniferous paleomagnetism. *Tectonophysics*, *366*, 113–141.

Bazhenov, M. L., Levashova, N. M., Degtyarev, K. E., Van der Voo, R., Abrajevitch, A. V., & McCausland, P. J. (2012). Unraveling the early–middle Paleozoic paleogeography of Kazakhstan on the basis of Ordovician and Devonian paleomagnetic results. *Gondwana Research*, *22*, 974–991.

Biske, Y. S., & Seltmann, R. (2010). Paleozoic Tian-Shan as a transitional region between the Rheic and Urals-Turkestan oceans. *Gondwana Research*, *17*, 602–613.

Bizimis, M., Salters, V. J. M., & Bonatti, E. (2000). Trace and REE content of clinopyroxenes from supra-subduction zone peridotites. Implications for melting and enrichment processes in island arcs. *Chemical Geology*, *165*, 67–85.

Cann, J. R. (1970). Rb, Sr, Y, Zr and Nb in some ocean floor basaltic rocks. *Earth and Planetary Science Letters*, *10*, 7–11.

Carroll, A. R., Graham, S. A., Chang, E. Z., & McKnight, C. (2001). Sinian through Permian tectonostratigraphic evolution of the northwestern Tarim basin, China. *Geological Society of America Memoirs*, *194*, 47–69.

Cawood, P. A., & Buchan, C. (2007). Linking accretionary orogenesis with supercontinent assembly. *Earth-Science Reviews*, *82*(3-4), 217–256. https://doi.org/10.1016/j.earscirev.2007.03.003

Cawood, P. A., Hawkesworth, C. J., & Dhuime, B. (2012). Detrital zircon record and tectonic setting. *Geology*, *40*, 875–878.

Cawood, P. A., Johnson, M. R. W., & Nemchin, A. A. (2007). Early Palaeozoic orogenesis along the Indian margin of Gondwana: Tectonic response to Gondwana assembly. *Earth and Planetary Science Letters*, *255*, 70–84.

Cawood, P. A., Kröner, A., Collins, W. J., Kusky, T. M., Mooney, W. D., & Windley, B. F. (2009). Accretionary orogens through Earth history. *Geological Society, London, Special Publications*, *318*, 1–36.

Charvet, J., Shu, L. S., Laurent-Charvet, S., Wang, B., Faure, M., Cluzel, D., et al. (2011). Palaeozoic tectonic evolution of the Tianshan belt, NW China. *Science China: Earth Sciences*, *54*, 166–184.

Chen, Y. B., Hu, A. Q., Zhang, G. X., & Zhang, Q. F. (2000). Zircon U–Pb age of granitic gneiss on Duku highway in western Tianshan of China and its geological implications. *Chinese Science Bulletin*, *45*, 649–653. (in Chinese with English abstract)

Choi, S. H., Shervais, J. W., & Mukasa, S. B. (2008). Supra-subduction and abyssal mantle peridotites of the Coast Range ophiolite, California. *Contributions to Mineralogy and Petrology*, *156*(5), 551–576. https://doi.org/10.1007/s00410-008-0300-6

Cocks, L. R. M., & Torsvik, T. H. (2013). The dynamic evolution of the Palaeozoic geography of eastern Asia. *Earth-Science Reviews*, *117*, 40–79.

Collins, A. S., & Pisarevsky, S. A. (2005). Amalgamating eastern Gondwana: The evolution of the Circum-Indian Orogens. *Earth-Science Reviews*, *71*, 229–270.

Corfu, F., Hanchar, J. M., Hoskin, P. W. O., & Kinny, P. (2003). Atlas of zircon textures. *Reviews in Mineralogy and Geochemistry*, *53*(1), 469–500. https://doi.org/10.2113/0530469

De Grave, J., Glorie, S., Buslov, M. M., Stockli, D. F., McWilliams, M. O., Batalev, V. Y., & Van den Haute, P. (2013). Thermo-tectonic history of the Issyk-Kul basement (Kyrgyz Northern Tien Shan, Central Asia). *Gondwana Research*, *23*, 998–1020.

Dewey, J. F. (1976). Ophiolite obduction. *Tectonophysics*, *31*(1-2), 93–120. https://doi.org/10.1016/0040-1951(76)90169-4

Dick, H. J. B. (1989). Abyssal peridotites, very slow spreading ridges and ocean ridge magmatism. *Geological Society, London, Special Publications*, *42*, 71–105.

Dick, H. J. B., & Natland, J. H. (1996). Late-stage melt evolution and transport in the shallow mantle beneath the East Pacific Rise, In: C. Mevel, K. M. Gillis, J. F. Allan, & P. S. Meyer (Eds.), Proceedings of Ocean Drilling Program, Scientific Results (pp. 103–134).

Dilek, Y., & Furnes, H. (2011). Ophiolite genesis and global tectonics: Geochemical and tectonic fingerprinting of ancient oceanic lithosphere. *Geological Society of America Bulletin*, *123*, 387–411.

Dilek, Y., & Furnes, H. (2014). Ophiolites and their origins. *Elements*, *10*, 93–100.

Ding, H. F., Ma, D. S., Yao, C. Y., & Shu, L. S. (2009). Sedimentary environment of Ediacaran glacigenic diamictite in Guozigou of Xinjiang, China. *Chinese Science Bulletin*, *54*(18), 3283–3294. https://doi.org/10.1007/s11434-009-0443-5

Dolgopolova, A., Seltmann, R., Konopelko, D., Biske, Y. S., Shatov, V., Armstrong, R., et al. (2017). Geodynamic evolution of the western Tien Shan, Uzbekistan: Insights from U–Pb SHRIMP geochronology and Sr–Nd–Pb–Hf isotope mapping of granitoids. *Gondwana Research*, *47*, 76–109.

Domeier, M. (2016). A plate tectonic scenario for the Iapetus and Rheic oceans. *Gondwana Research*, *36*, 275–295.

Domeier, M., & Torsvik, T. H. (2014). Plate tectonics in the late Paleozoic. *Geoscience Frontiers*, *5*, 303–350.

Dong, Y. P., Zhou, D. W., Zhang, G. W., Zhang, C. L., Xia, L. Q., Xue, X. Y., & Li, X. M. (2005). Tectonic setting of the Wuwamen ophiolite at the southern margin of Middle Tianshan Belt. *Acta Petrologica Sinica*, *21*, 37–44. (in Chinese with English abstract)

Edwards, S. J., & Malpas, J. (1996). Melt-peridotite interactions in shallow mantle at the East Pacific Rise: Evidence from ODP Site 895 (Hess Deep). *Mineralogical Magazine*, *60*, 191–206.

Eizenhöfer, P. R., & Zhao, G. C. (2017). Solonker Suture in East Asia and its bearing on the final closure of the eastern segment of the Palaeo-Asian Ocean. *Earth-Science Reviews*. https://doi.org/10.1016/j.earscirev.2017.1009.1010

Gao, J., & Klemd, R. (2003). Formation of HP–LT rocks and their tectonic implications in the western Tianshan Orogen, NW China: Geochemical and age constraints. *Lithos*, *66*, 1–22.

Gao, J., Klemd, R., Qian, Q., Zhang, X., Li, J. L., Jiang, T., & Yang, Y. Q. (2011). The collision between the Yili and Tarim blocks of the Southwestern Altaids: Geochemical and age constraints of a leucogranite dike crosscutting the HP–LT metamorphic belt in the Chinese Tianshan Orogen. *Tectonophysics*, *499*(1-4), 118–131. https://doi.org/10.1016/j.tecto.2011.01.001

Gao, J., Li, M. S., Xiao, X. C., Tang, Y. Q., & He, G. Q. (1998). Paleozoic tectonic evolution of the Tianshan Orogen, northwestern China. *Tectonophysics*, *287*, 213–231.

Gao, J., Long, L. L., Klemd, R., Qian, Q., Liu, D. Y., Xiong, X. M., et al. (2009). Tectonic evolution of the South Tianshan orogen and adjacent regions, NW China: Geochemical and age constraints of granitoid rocks. *International Journal of Earth Sciences*, *98*, 1221–1238.

Gao, J., Wang, X. S., Klemd, R., Jiang, T., Qian, Q., Mu, L. X., & Ma, Y. Z. (2015). Record of assembly and breakup of Rodinia in the Southwestern Altaids: Evidence from Neoproterozoic magmatism in the Chinese Western Tianshan Orogen. *Journal of Asian Earth Sciences*, *113*, 173–193.

Ge, R. F., Zhu, W. B., & Wilde, S. A. (2016). Mid-Neoproterozoic (ca. 830–800 Ma) metamorphic P–T paths link Tarim to the circum-Rodinia subduction-accretion system. *Tectonics*, *35*, 1465–1488. https://doi.org/10.1002/2016TC004177

Ge, R. F., Zhu, W. B., Wilde, S. A., He, J. W., Cui, X., Wang, X., & Zheng, B. H. (2014). Neoproterozoic to Paleozoic long-lived accretionary orogeny in the northern Tarim Craton. *Tectonics*, *33*, 302–329. https://doi.org/10.1002/2013TC003501

Ge, R. F., Zhu, W. B., Wilde, S. A., Wu, H. L., He, J. W., & Zheng, B. H. (2014). Archean magmatism and crustal evolution in the northern Tarim Craton: Insights from zircon U–Pb–Hf–O isotopes and geochemistry of ~2.7 Ga orthogneiss and amphibolite in the Korla Complex. *Precambrian Research*, *252*, 145–165.

Ge, R. F., Zhu, W. B., Wu, H. L., He, J. W., & Zheng, B. H. (2013). Zircon U–Pb ages and Lu–Hf isotopes of Paleoproterozoic metasedimentary rocks in the Korla Complex, NW China: Implications for metamorphic zircon formation and geological evolution of the Tarim Craton. *Precambrian Research*, *231*, 1–18. https://doi.org/10.1016/j.precamres.2013.03.003

Ge, R. F., Zhu, W. B., Wu, H. L., Zheng, B. H., Zhu, X. Q., & He, J. W. (2012). The Paleozoic northern margin of the Tarim Craton: Passive or active? *Lithos*, *142*, 1–15.

Ge, R. F., Zhu, W. B., Zheng, B. H., Wu, H. L., He, J. W., & Zhu, X. Q. (2012). Early Pan-African magmatism in the Tarim Craton: Insights from zircon U–Pb–Lu–Hf isotope and geochemistry of granitoids in the Korla area, NW China. *Precambrian Research*, *212–213*, 117–138.

Glorie, S., De Grave, J., Buslov, M. M., Elburg, M. A., Stockli, D. F., & Gerdes, A. (2010). Multi-method chronometric constraints on the evolution of the Northern Kyrgyz Tien Shan granitoids (Central Asian Orogenic Belt): From emplacement to exhumation. *Journal of Asian Earth Sciences*, *38*(3-4), 131–146. https://doi.org/10.1016/j.jseaes.2009.12.009

Glorie, S., De Grave, J., Buslov, M. M., Zhimulev, F. I., Stockli, D. F., Batalev, V. Y., et al. (2011). Tectonic history of the Kyrgyz South Tien Shan (Atbashi-Inylchek) suture zone: The role of inherited structures during deformation-propagation. *Tectonics*, *30*, TC6016. https://doi.org/10.1029/2011TC002949

Goldstein, S. L., O'Nions, R. K., & Hamilton, P. J. (1984). A Sm–Nd isotopic study of atmospheric dusts and particulates from major river systems. *Earth and Planetary Science Letters*, *70*(2), 221–236. https://doi.org/10.1016/0012-821X(84)90007-4

Han, B. F., Guo, Z. J., Zhang, Z. C., Zhang, L., Chen, J. F., & Song, B. (2010). Age, geochemistry, and tectonic implications of a late Paleozoic stitching pluton in the North Tian Shan suture zone, western China. *Geological Society of America Bulletin*, *122*(3-4), 627–640. https://doi.org/10.1130/B26491.1

Han, B. F., He, G. Q., Wang, X. C., & Guo, Z. J. (2011). Late Carboniferous collision between the Tarim and Kazakhstan–Yili terranes in the western segment of the South Tian Shan Orogen, Central Asia, and implications for the Northern Xinjiang, western China. *Earth-Science Reviews*, *109*(3-4), 74–93. https://doi.org/10.1016/j.earscirev.2011.09.001

Han, Y. G., & Zhao, G. C. (2017). Final amalgamation of the Tianshan and Junggar orogenic collage in the southwestern Central Asian Orogenic Belt: Constraints on the closure of the Paleo-Asian Ocean. *Earth-Science Reviews*. https://doi.org/10.1016/j.earscirev.2017.1009.1012

Han, Y. G., Zhao, G. C., Cawood, P. A., Sun, M., Eizenhöfer, P. R., Hou, W. Z., et al. (2016). Tarim and North China cratons linked to northern Gondwana through switching accretionary tectonics and collisional orogenesis. *Geology*, *44*, 95–98.

Han, Y. G., Zhao, G. C., Sun, M., Eizenhöfer, P. R., Hou, W. Z., Zhang, X. R., et al. (2015). Paleozoic accretionary orogenesis in the Paleo-Asian Ocean: Insights from detrital zircons from Silurian to Carboniferous strata at the northwestern margin of the Tarim Craton. *Tectonics*, *34*, 334–351. https://doi.org/10.1002/2014TC003668

Han, Y. G., Zhao, G. C., Sun, M., Eizenhöfer, P. R., Hou, W. Z., Zhang, X. R., et al. (2016). Late Paleozoic subduction and collision processes during the amalgamation of the Central Asian Orogenic Belt along the South Tianshan suture zone. *Lithos*, *246–247*, 1–12.

Haschke, M., Siebel, W., Günther, A., & Scheuber, E. (2002). Repeated crustal thickening and recycling during the Andean orogeny in north Chile (21°–26°S). *Journal of Geophysical Research*, *107*(B1), 2019. https://doi.org/10.1029/2001JB000328

He, Z. Y., Zhang, Z. M., Zong, K. Q., Wang, W., & Santosh, M. (2012). Neoproterozoic granulites from the northeastern margin of the Tarim Craton: Petrology, zircon U–Pb ages and implications for the Rodinia assembly. *Precambrian Research*, *212*, 21–33.

Hegner, E., Klemd, R., Kröner, A., Corsini, M., Alexeiev, D. V., Iaccheri, L. M., et al. (2010). Mineral ages and P–T conditions of late Paleozoic high-pressure eclogite and provenance of mélange sediments from Atbashi in the south Tianshan orogen of Kyrgyzstan. *American Journal of Science*, *310*, 916–950.

Hellebrand, E., Snow, J. E., Dick, H. J. B., & Hofmann, A. W. (2001). Coupled major and trace elements as indicators of the extent of melting in mid-ocean-ridge peridotites. *Nature*, *410*(6829), 677–681. https://doi.org/10.1038/35070546

Hermann, J., Rubatto, D., Korsakov, A., & Shatsky, V. S. (2001). Multiple zircon growth during fast exhumation of diamondiferous, deeply subducted continental crust (Kokchetav Massif, Kazakhstan). *Contributions to Mineralogy and Petrology*, *141*, 66–82.

Hoskin, P. W. O. (2005). Trace-element composition of hydrothermal zircon and the alteration of Hadean zircon from the Jack Hills, Australia. *Geochimica et Cosmochimica Acta*, *69*(3), 637–648. https://doi.org/10.1016/j.gca.2004.07.006

Huang, H., Zhang, Z. C., Santosh, M., & Zhang, D. Y. (2014). Geochronology, geochemistry and metallogenic implications of the Boziguo'er rare metal-bearing peralkaline granitic intrusion in South Tianshan, NW China. *Ore Geology Reviews*, *61*, 157–174.

Huang, H., Zhang, Z. C., Santosh, M., Zhang, D. Y., & Wang, T. (2015). Petrogenesis of the early Permian volcanic rocks in the Chinese South Tianshan: Implications for crustal growth in the Central Asian Orogenic Belt. *Lithos*, *228*, 23–42.

Huang, H., Zhang, Z. C., Santosh, M., Zhang, D. Y., Zhao, Z. D., & Liu, J. L. (2013). Early Paleozoic tectonic evolution of the South Tianshan Collisional Belt: Evidence from geochemistry and zircon U–Pb geochronology of the Tie'reke monzonite pluton, Northwest China. *The Journal of Geology*, *121*, 401–424.

Jian, P., Kröner, A., Jahn, B. M., Liu, D. Y., Zhang, W., Shi, Y. R., & Ma, H. D. (2013). Zircon ages of metamorphic and magmatic rocks within peridotite-bearing mélanges: Crucial time constraints on early Carboniferous extensional tectonics in the Chinese Tianshan. *Lithos*, *172*, 243–266.

Jiang, T., Gao, J., Klemd, R., Qian, Q., Zhang, X., Wang, X. S., et al. (2015). Genetically and geochronologically contrasting plagiogranites in South Central Tianshan ophiolitic mélange: Implications for the breakup of Rodinia and subduction zone processes. *Journal of Asian Earth Sciences*, *113*, 266–281.

Jiang, T., Gao, J., Klemd, R., Qian, Q., Zhang, X., Xiong, X. M., et al. (2014). Paleozoic ophiolitic mélanges from the South Tianshan Orogen, NW China: Geological, geochemical and geochronological implications for the geodynamic setting. *Tectonophysics*, *612*, 106–127.

Kang, J. L., Zhang, Z. C., Dong, S. Y., Ma, L. T., Zhang, S., Zhang, D. Y., & Huang, H. (2010). Geochemistry of cherts from Madaer area in Southwest Tianshan Mountains: Implications for deposition environments. *Acta Petrologica et Mineralogica*, *29*, 79–89. (in Chinese with English abstract)

Klemd, R., Bröcker, M., Hacker, B. R., Gao, J., Gans, P., & Wemmer, K. (2005). New age constraints on the metamorphic evolution of the high-pressure/low-temperature belt in the Western Tianshan Mountains, NW China. *The Journal of Geology*, *113*(2), 157–168. https://doi.org/10.1086/427666

Klemd, R., Gao, J., Li, J. L., & Meyer, M. (2015). Metamorphic evolution of (ultra)-high-pressure subduction-related transient crust in the South Tianshan Orogen (Central Asian Orogenic Belt): Geodynamic implications. *Gondwana Research*, *28*, 1–25.

Klemd, R., Hegner, E., Bergmann, H., Pfänder, J. A., Li, J. L., & Hentschel, F. (2014). Eclogitization of transient crust of the Aktyuz Complex during late Palaeozoic plate collisions in the Northern Tianshan of Kyrgyzstan. *Gondwana Research*, *26*, 925–941.

Klemd, R., John, T., Scherer, E. E., Rondenay, S., & Gao, J. (2011). Changes in dip of subducted slabs at depth: Petrological and geochronological evidence from HP–UHP rocks (Tianshan, NW-China). *Earth and Planetary Science Letters*, *310*, 9–20.

Konopelko, D., Biske, G., Seltmann, R., Eklund, O., & Belyatsky, B. (2007). Hercynian post-collisional A-type granites of the Kokshaal Range, southern Tien Shan, Kyrgyzstan. *Lithos*, *97*(1-2), 140–160. https://doi.org/10.1016/j.lithos.2006.12.005

Konopelko, D., Biske, G., Seltmann, R., Petrov, S. V., & Lepekhina, E. (2014). Age and petrogenesis of the Neoproterozoic Chon-Ashu alkaline complex, and a new discovery of chalcopyrite mineralization in the eastern Kyrgyz Tien Shan. *Ore Geology Reviews*, *61*, 175–191. https://doi.org/10.1016/j.oregeorev.2014.02.004

Konopelko, D., Kullerud, K., Apayarov, F., Sakiev, K., Baruleva, O., Ravna, E., & Lepekhina, E. (2012). SHRIMP zircon chronology of HP–UHP rocks of the Makbal metamorphic complex in the Northern Tien Shan, Kyrgyzstan. *Gondwana Research*, *22*, 300–309.

Konopelko, D., Seltmann, R., Apayarov, F., Belousova, E., Izokh, A., & Lepekhina, E. (2013). U–Pb–Hf zircon study of two mylonitic granite complexes in the Talas-Fergana fault zone, Kyrgyzstan, and Ar–Ar age of deformations along the fault. *Journal of Asian Earth Sciences*, *73*, 334–346.

Konopelko, D., Seltmann, R., Mamadjanov, Y., Romer, R. L., Rojas-Agramonte, Y., Jeffries, T., et al. (2017). A geotraverse across two paleo-subduction zones in Tien Shan, Tajikistan. *Gondwana Research*, *47*, 110–130.

Kroner, U., & Romer, R. L. (2010). The Saxo-Thuringian Zone—tip of the Armorican Spur and part of the Gondwana plate. In U. Linnemann & R. L. Romer (Eds.), *Pre-Mesozoic Geology of Saxo-Thuringia—From the Cadomian Active Margin to the Variscan Orogen* (pp. 371–394). Stuttgart: Schweizerbart.

Kröner, A., Alexeiev, D. V., Hegner, E., Rojas-Agramonte, Y., Corsini, M., Chao, Y., et al. (2012). Zircon and muscovite ages, geochemistry, and Nd–Hf isotopes for the Aktyuz metamorphic terrane: Evidence for an Early Ordovician collisional belt in the northern Tianshan of Kyrgyzstan. *Gondwana Research*, *21*(4), 901–927. https://doi.org/10.1016/j.gr.2011.05.010

Kröner, A., Alexeiev, D. V., Kovach, V. P., Rojas-Agramonte, Y., Tretyakov, A. A., Mikolaichuk, A. V., et al. (2017). Zircon ages, geochemistry and Nd isotopic systematics for the Palaeoproterozoic 2.3–1.8 Ga Kuilyu Complex, East Kyrgyzstan–the oldest continental basement fragment in the Tianshan orogenic belt. *Journal of Asian Earth Sciences*, *135*, 122–135.

Kröner, A., Alexeiev, D. V., Rojas-Agramonte, Y., Hegner, E., Wong, J., Xia, X., et al. (2013). Mesoproterozoic (Grenville-age) terranes in the Kyrgyz North Tianshan: Zircon ages and Nd–Hf isotopic constraints on the origin and evolution of basement blocks in the southern Central Asian Orogen. *Gondwana Research*, *23*, 272–295.

Kröner, A., Windley, B. F., Badarch, G., Tomurtogoo, O., Hegner, E., Jahn, B. M., et al. (2007). Accretionary growth and crust formation in the Central Asian Orogenic Belt and comparison with the Arabian-Nubian shield. *Geological Society of America Memoirs*, *200*, 181–209.

Kuibida, M. L., Safonova, I. Y., Yermolov, P. V., Vladimirov, A. G., Kruk, N. N., & Yamamoto, S. (2016). Tonalites and plagiogranites of the Char suture-shear zone in East Kazakhstan: Implications for the Kazakhstan-Siberia collision. *Geoscience Frontiers*, *7*, 141–150.

Le Bas, M. J., Le Maitre, R. W., Streckeisen, A., & Zanettin, B. (1986). A chemical classification of volcanic rocks based on the total alkali-silica diagram. *Journal of Petrology*, *27*(3), 745–750. https://doi.org/10.1093/petrology/27.3.745

Levashova, N. M., Meert, J. G., Gibsher, A. S., Grice, W. C., & Bazhenov, M. L. (2011). The origin of microcontinents in the Central Asian Orogenic Belt: Constraints from paleomagnetism and geochronology. *Precambrian Research*, *185*(1-2), 37–54. https://doi.org/10.1016/j.precamres.2010.12.001

Li, D., He, D. F., Santosh, M., & Tang, J. Y. (2014). Petrogenesis of late Paleozoic volcanics from the Zhaheba depression, East Junggar: Insights into collisional event in an accretionary orogen of Central Asia. *Lithos*, *184–187*, 167–193.

Li, J. L., Gao, J., & Wang, X. S. (2016). A subduction channel model for exhumation of oceanic-type high-pressure to ultrahigh-pressure eclogite-facies metamorphic rocks in SW Tianshan, China. *Science China Earth Sciences*, *59*, 2339–2354.

Li, P. F., Sun, M., Rosenbaum, G., Jourdan, F., Li, S. Z., & Cai, K. D. (2017). Late Paleozoic closure of the Ob-Zaisan Ocean along the Irtysh shear zone (NW China): Implications for arc amalgamation and oroclinal bending in the Central Asian orogenic belt. *Geological Society of America Bulletin*, *129*, 547–569.

Li, P. F., Sun, M., Rosenbaum, G., Yuan, C., Safonova, I., Cai, K. D., et al. (2018). Geometry, kinematics and tectonic models of the Kazakhstan Orocline, Central Asian Orogenic Belt. *Journal of Asian Earth Sciences*, *153*, 42–56.

Lin, W., Chu, Y., Ji, W. B., Zhang, Z. P., Shi, Y. H., Wang, Z. Y., et al. (2013). Geochronological and geochemical constraints for a middle Paleozoic continental arc on the northern margin of the Tarim block: Implications for the Paleozoic tectonic evolution of the South Chinese Tianshan. *Lithosphere*, *5*(4), 355–381. https://doi.org/10.1130/L231.1

Lin, W., Faure, M., Shi, Y., Wang, Q., & Li, Z. (2009). Palaeozoic tectonics of the south-western Chinese Tianshan: New insights from a structural study of the high-pressure/low-temperature metamorphic belt. *International Journal of Earth Sciences*, *98*, 1259–1274.

Liu, B., Han, B. F., Xu, Z., Ren, R., Zhang, J. R., Zhou, J., et al. (2016). The Cambrian initiation of intra-oceanic subduction in the southern Paleo-Asian Ocean: Further evidence from the Barleik subduction-related metamorphic complex in the West Junggar region, NW China. *Journal of Asian Earth Sciences*, *123*, 1–21.

Liu, C. Z., Zhang, C., Xu, Y., Wang, J. G., Chen, Y., Guo, S., et al. (2016). Petrology and geochemistry of mantle peridotites from the Kalaymyo and Myitkyina ophiolites (Myanmar): Implications for tectonic settings. *Lithos*, *264*, 495–508.

Liu, D. D., Guo, Z. J., Jolivet, M., Cheng, F., Song, Y., & Zhang, Z. Y. (2014). Petrology and geochemistry of early Permian volcanic rocks in South Tian Shan, NW China: Implications for the tectonic evolution and Phanerozoic continental growth. *International Journal of Earth Sciences*, *103*, 737–756.

Liu, H. S., Wang, B., Shu, L. S., Jahn, B. M., & Lizuka, Y. (2014). Detrital zircon ages of Proterozoic meta-sedimentary rocks and Paleozoic sedimentary cover of the northern Yili Block: Implications for the tectonics of microcontinents in the Central Asian Orogenic Belt. *Precambrian Research*, *252*, 209–222. https://doi.org/10.1016/j.precamres.2014.07.018

Liu, Y., Wang, N. W., & Yao, J. X. (1994). New data of radiolaria and its significance in the Kuqa area, Xinjiang. *Xinjiang Geology*, *12*, 344–351. (in Chinese with English abstract)

Lomize, M. G., Demina, L. I., & Zarshchikov, A. A. (1997). The Kyrgyz-Terskei Paleoceanic Basin, Tien Shan. *Geotectonics*, *31*, 463–482.

Long, L. L., Gao, J., Klemd, R., Beier, C., Qian, Q., Zhang, X., et al. (2011). Geochemical and geochronological studies of granitoid rocks from the Western Tianshan Orogen: Implications for continental growth in the southwestern Central Asian Orogenic Belt. *Lithos*, *126*, 321–340.

Long, L. L., Gao, J., Xiong, X. M., & Qian, Q. (2006). The geochemical characteristics and age of the Kule Lake ophiolite in the southern Tianshan. *Acta Petrologica Sinica*, *22*, 65–73. (in Chinese with English abstract)

Loury, C., Rolland, Y., Cenki-Tok, B., Lanari, P., & Guillot, S. (2016). Late Paleozoic evolution of the South Tien Shan: Insights from P–T estimates and allanite geochronology on retrogressed eclogites (Chatkal range, Kyrgyzstan). *Journal of Geodynamics*, *96*, 62–80. https://doi.org/10.1016/j.jog.2015.06.005

Loury, C., Rolland, Y., Guillot, S., Mikolaichuk, A. V., Lanari, P., Bruguier, O., & Bosch, D. (2015). Crustal-scale structure of South Tien Shan: Implications for subduction polarity and Cenozoic reactivation. *Geological Society, London, Special Publications*, *427*, 197–229.

Lu, S. N., Li, H. K., Zhang, C. L., & Niu, G. H. (2008). Geological and geochronological evidence for the Precambrian evolution of the Tarim Craton and surrounding continental fragments. *Precambrian Research*, *160*(1-2), 94–107. https://doi.org/10.1016/j.precamres.2007.04.025

Ma, X. X., Shu, L. S., Santosh, M., & Li, J. Y. (2012). Petrogenesis and tectonic significance of an early Palaeozoic mafic-intermediate suite of rocks from the Central Tianshan, Northwest China. *International Geology Review*, *55*, 548–573.

Ma, Z. P., Xia, L. Q., Xu, X. Y., Li, X. M., Xia, Z. C., & Wang, L. S. (2007). Dating for zircons of gabbro from Kulehu ophiolite, southern Tianshan, and its geological implication. *Journal of Northwest University*, *37*, 107–110. (in Chinese with English abstract)

Metcalfe, I. (2013). Gondwana dispersion and Asian accretion: Tectonic and palaeogeographic evolution of eastern Tethys. *Journal of Asian Earth Sciences*, *66*, 1–33.

Meyer, M., Klemd, R., Hegner, E., & Konopelko, D. (2014). Subduction and exhumation mechanisms of ultra-high and high-pressure oceanic and continental crust at Makbal (Tianshan, Kazakhstan and Kyrgyzstan). *Journal of Metamorphic Geology*, *32*, 861–884.

Mirkamalov, R. K., Chirikin, V. V., Khan, R. S., Kharin, V. G., & Sergeev, S. A. (2012). Results of U–Pb (SHRIMP) dating of granitoid and metamorphic complexes of the Tien Shan Foldbelt (Uzbekistan). *Vestnik St.-Petersburg University Series*, *7*, 3–25. (in Russian)

Miyashiro, A. (1973). The Troodos ophiolitic complex was probably formed in an island arc. *Earth and Planetary Science Letters*, *19*, 218–224.

Mühlberg, M., Hegner, E., Klemd, R., Pfänder, J. A., Kaliwoda, M., & Biske, Y. S. (2016). Late Carboniferous high-pressure metamorphism of the Kassan Metamorphic Complex (Kyrgyz Tianshan) and assembly of the SW Central Asian Orogenic Belt. *Lithos*, *264*, 41–55.

Parkinson, I. J., & Pearce, J. A. (1998). Peridotites from the Izu–Bonin–Mariana Forearc (ODP Leg 125): Evidence for mantle melting and melt–mantle interaction in a supra-subduction zone setting. *Journal of Petrology*, *39*, 1577–1618.

Pearce, J. A. (2008). Geochemical fingerprinting of oceanic basalts with applications to ophiolite classification and the search for Archean oceanic crust. *Lithos*, *100*(1-4), 14–48. https://doi.org/10.1016/j.lithos.2007.06.016

Pearce, J. A. (2014). Immobile element fingerprinting of ophiolites. *Elements*, *10*(2), 101–108. https://doi.org/10.2113/gselements.10.2.101

Pearce, J. A., Barker, P. F., Edwards, S. J., Parkinson, I. J., & Leat, P. T. (2000). Geochemistry and tectonic significance of peridotites from the South Sandwich arc–basin system, South Atlantic. *Contributions to Mineralogy and Petrology*, *139*, 36–53.

Puchkov, V. N. (1997). Structure and geodynamics of the Uralian orogen. *Geological Society, London, Special Publications*, *121*(1), 201–236. https://doi.org/10.1144/GSL.SP.1997.121.01.09

Qian, Q., Gao, J., Klemd, R., He, G. Q., Song, B., Liu, D. Y., & Xu, R. H. (2009). Early Paleozoic tectonic evolution of the Chinese South Tianshan Orogen: Constraints from SHRIMP zircon U–Pb geochronology and geochemistry of basaltic and dioritic rocks from Xiate, NW China. *International Journal of Earth Sciences*, *98*, 551–569.

Rojas-Agramonte, Y., Herwartz, D., García-Casco, A., Kröner, A., Alexeiev, D. V., Klemd, R., et al. (2013). Early Palaeozoic deep subduction of continental crust in the Kyrgyz North Tianshan: Evidence from Lu–Hf garnet geochronology and petrology of mafic dikes. *Contributions to Mineralogy and Petrology*, *166*, 525–543.

Ryazantsev, A. V., Degtyarev, K. E., Kotov, A. B., Sal'nikova, E. B., Anisimova, I. V., & Yakovleva, S. Z. (2009). Ophiolite sections of the Dzhalair-Nayman zone, South Kazakhstan: Their structure and age substantiation. *Doklady Earth Sciences*, *427*, 902–906.

Safonova, I., Biske, G., Romer, R. L., Seltmann, R., Simonov, V., & Maruyama, S. (2016). Middle Paleozoic mafic magmatism and ocean plate stratigraphy of the South Tianshan, Kyrgyzstan. *Gondwana Research*, *30*, 236–256.

Sang, M., Xiao, W. J., Orozbaev, R., Bakirov, A., Sakiev, K., Pak, N., et al. (2018). Structural styles and zircon ages of the South Tianshan accretionary complex, Atbashi Ridge, Kyrgyzstan: Insights for the anatomy of ocean plate stratigraphy and accretionary processes. *Journal of Asian Earth Sciences*, *153*, 9–41. https://doi.org/10.1016/j.jseaes.2017.07.052

Seltmann, R., Konopelko, D., Biske, G., Divaev, F., & Sergeev, S. (2011). Hercynian post-collisional magmatism in the context of Paleozoic magmatic evolution of the Tien Shan orogenic belt. *Journal of Asian Earth Sciences*, *42*(5), 821–838. https://doi.org/10.1016/j.jseaes.2010.08.016

Sengör, A. M. C., Natal'in, B. A., & Burtman, V. S. (1993). Evolution of the Altaid tectonic collage and Paleozoic crustal growth in Eurasia. *Nature*, *364*, 299–307.

Stampfli, G. M., Hochard, C., Vérard, C., Wilhem, C., & vonRaumer, J. (2013). The formation of Pangea. *Tectonophysics*, *593*, 1–19.

Su, W., Gao, J., Klemd, R., Li, J. L., Zhang, X., Li, X. H., et al. (2010). U–Pb zircon geochronology of Tianshan eclogites in NW China: Implication for the collision between the Yili and Tarim blocks of the southwestern Altaids. *European Journal of Mineralogy*, *22*, 473–478.

Sun, S. S., & McDonough, W. F. (1989). Chemical and isotopic systematics of oceanic basalts: Implications for mantle composition and processes. In A. D. Saunders & M. J. Norry (Eds.), *Magmatism in the Ocean Basin*, *Special Publications* (pp. 313–345). London: Geological Society.

Tan, Z., Agard, P., Gao, J., John, T., Li, J. L., Jiang, T., et al. (2017). P–T–time-isotopic evolution of coesite-bearing eclogites: Implications for exhumation processes in SW Tianshan. *Lithos*, *278–281*, 1–25.

Volkova, N. I., & Budanov, V. I. (1999). Geochemical discrimination of metabasalt rocks of the fan–Karategin transitional blueschist/greenschist belt, south Tianshan, Tajikistan: Seamount volcanism and accretionary tectonics. *Lithos*, *47*, 201–216.

von Raumer, J. F., Stampfli, G. M., & Bussy, F. (2003). Gondwana-derived microcontinents—The constituents of the Variscan and Alpine collisional orogens. *Tectonophysics*, *365*, 7–22.

Wang, B., Chen, B., Ji, W. H., Hong, J., Yang, B., Meng, G. L., & Cao, J. F. (2016). Geological features of Djanydjer ophiolitic mélange and chronology of gabbro in Kyrgyz, South Tianshan. *Earth Science Frontiers*, *23*, 198–209. (in Chinese with English abstract)

Wang, B., Faure, M., Shu, L. S., Cluzel, D., Charvet, J., De Jong, K., & Chen, Y. (2008). Paleozoic tectonic evolution of the Yili Block, western Chinese Tianshan. *Bulletin de la Societe Geologique de France*, *179*, 483–490.

Wang, B., Faure, M., Shu, L. S., de Jong, K., Charvet, J., Cluzel, D., et al. (2010). Structural and geochronological study of high-pressure metamorphic rocks in the Kekesu section (northwestern China): Implications for the late Paleozoic tectonics of the Southern Tianshan. *The Journal of Geology*, *118*, 59–77.

Wang, B., Liu, H. S., Shu, L. S., Jahn, B. M., Chung, S. L., Zhai, Y. Z., & Liu, D. Y. (2014). Early Neoproterozoic crustal evolution in northern Yili Block: Insights from migmatite, orthogneiss and leucogranite of the Wenquan metamorphic complex in the NW Chinese Tianshan. *Precambrian Research*, *242*, 58–81. https://doi.org/10.1016/j.precamres.2013.12.006

Wang, B., Shu, L. S., Faure, M., Jahn, B. M., Cluzel, D., Charvet, J., et al. (2011). Paleozoic tectonics of the southern Chinese Tianshan: Insights from structural, chronological and geochemical studies of the Heiyingshan ophiolitic mélange (NW China). *Tectonophysics*, *497*, 85–104.

Wang, B., Shu, L. S., Liu, H. S., Gong, H. J., Ma, Y. Z., Mu, L. X., & Zhong, L. L. (2014). First evidence for ca. 780 Ma intra-plate magmatism and its implications for Neoproterozoic rifting of the North Yili Block and tectonic origin of the continental blocks in SW of Central Asia. *Precambrian Research*, *254*, 258–272.

Wang, B., Zhai, Y. Z., Kapp, P., de Jong, K., Zhong, L. L., Liu, H. S., et al. (2017). Accretionary tectonics of back-arc oceanic basins in the South Tianshan: Insights from structural, geochronological, and geochemical studies of the Wuwamen ophiolite mélange. *Geological Society of America Bulletin*, *130*, 284–306.

Wang, C., Liu, L., Che, Z. C., Luo, J. H., & Zhang, J. Y. (2007). Geochronology, Petrogenesis and significance of Baleigong mafic rocks in Kokshal segment, southwestern Tianshan Mountains. *Geological Review*, *53*, 743–754. (in Chinese with English abstract)

Wang, X. S., Gao, J., Klemd, R., Jiang, T., Li, J. L., Zhang, X., et al. (2014). Geochemistry and geochronology of the Precambrian high-grade metamorphic complex in the Southern Central Tianshan ophiolitic mélange, NW China. *Precambrian Research*, *254*, 129–148.

Wang, X. S., Gao, J., Klemd, R., Jiang, T., Li, J. L., Zhang, X., & Xue, S. C. (2017). The Central Tianshan Block: A microcontinent with a Neoarchean-Paleoproterozoic basement in the southwestern Central Asian Orogenic Belt. *Precambrian Research*, *295*, 130–150.

Wang, X. S., Gao, J., Klemd, R., Jiang, T., Zhai, Q. G., Xiao, X. C., & Liang, X. Q. (2015). Early Neoproterozoic multiple arc–back-arc system formation during subduction–accretion processes between the Yangtze and Cathaysia blocks: New constraints from the supra-subduction zone NE Jiangxi ophiolite (South China). *Lithos*, *236*, 90–105.

Wang, X. S., Zhang, X., Gao, J., Li, J. L., Jiang, T., & Xue, S. C. (2018). A slab break-off model for the submarine volcanic-hosted iron mineralization in the Chinese Western Tianshan: Insights from Paleozoic subduction-related to post-collisional magmatism. *Ore Geology Reviews*, *92*, 144–160.

Wang, Y., Huang, H., Zhang, D. Y., Zhang, Z. C., Encarnacion, J., & Zhao, L. (2012). SHRIMP dating of the Qiqijianake ophiolitic melange in the Kokshal region, southwestern Tianshan and its tectonic implications. *Acta Petrologica Sinica*, *28*, 1273–1281. (in Chinese with English abstract)

Wilhem, C., Windley, B. F., & Stampfli, G. M. (2012). The Altaids of Central Asia: A tectonic and evolutionary innovative review. *Earth-Science Reviews*, *113*, 303–341.

Winchester, J. A., & Floyd, P. A. (1977). Geochemical discrimination of different magma series and their differentiation products using immobile elements. *Chemical Geology*, *20*, 325–343.

Windley, B. F., Alexeiev, D., Xiao, W. J., Kröner, A., & Badarch, G. (2007). Tectonic models for accretion of the Central Asian Orogenic Belt. *Journal of the Geological Society, London*, *164*(1), 31–47. https://doi.org/10.1144/0016-76492006-022

Windley, B. F., Allen, M. B., Zhang, C., Zhao, Z. Y., & Wang, G. R. (1990). Paleozoic accretion and Cenozoic redeformation of the Chinese Tien Shan range, Central Asia. *Geology*, *18*, 128–131.

Wood, D. A. (1980). The application of a Th–Hf–Ta diagram to problems of tectonomagmatic classification and to establishing the nature of crustal contamination of basaltic lavas of the British Tertiary volcanic province. *Earth and Planetary Science Letters*, *50*, 11–30.

Workman, R. K., & Hart, S. R. (2005). Major and trace element composition of the depleted MORB mantle (DMM). *Earth and Planetary Science Letters*, *231*, 53–72.

Worthington, J. R., Kapp, P., Minaev, V., Chapman, J. B., Mazdab, F. K., Ducea, M. N., et al. (2017). Birth, life, and demise of the Andean–syn-collisional Gissar arc: Late Paleozoic tectono-magmatic-metamorphic evolution of the southwestern Tian Shan, Tajikistan. *Tectonics*, *36*, 1861–1912. https://doi.org/10.1002/2016TC004285

Xia, B., Zhang, L. F., & Bader, T. (2014). Zircon U–Pb ages and Hf isotopic analyses of migmatite from the 'paired metamorphic belt' in Chinese SW Tianshan: Constraints on partial melting associated with orogeny. *Lithos*, *192–195*, 158–179.

Xiao, W. J., Huang, B. C., Han, C. M., Sun, S., & Li, J. L. (2010). A review of the western part of the Altaids: A key to understanding the architecture of accretionary orogens. *Gondwana Research*, *18*, 253–273.

Xiao, W. J., Windley, B. F., Allen, M. B., & Han, C. M. (2013). Paleozoic multiple accretionary and collisional tectonics of the Chinese Tianshan orogenic collage. *Gondwana Research*, *23*, 1316–1341.

Xiao, W. J., Windley, B. F., Sun, S., Li, J. L., Huang, B. C., Han, C. M., et al. (2015). A tale of amalgamation of three Permo-Triassic collage systems in Central Asia: Oroclines, sutures, and terminal accretion. *Annual Review of Earth and Planetary Sciences*, *43*, 477–507.

Xu, B., Charvet, J., Chen, Y., Zhao, P., & Shi, G. (2013). Middle Paleozoic convergent orogenic belts in western Inner Mongolia (China): Framework, kinematics, geochronology and implications for tectonic evolution of the Central Asian Orogenic Belt. *Gondwana Research*, *23*, 1342–1364.

Xu, B., Xiao, S. H., Zou, H. B., Chen, Y., Li, Z. X., Song, B., et al. (2009). SHRIMP zircon U–Pb age constraints on Neoproterozoic Quruqtagh diamictites in NW China. *Precambrian Research*, *168*, 247–258.

Xu, X. Y., Ma, Z. P., Li, X. M., He, S. P., & Yang, J. L. (2003). The discovery of P-MORB in Jigen area of southwest Tianshan Mountains and its tectonic implications. *Acta Petrologica et Mineralogica*, *22*, 245–253. (in Chinese with English abstract)

Xu, X. Y., Xia, L. Q., Ma, Z. P., Wang, Y. B., Xia, Z. C., Li, X. M., & Wang, L. S. (2006). SHRIMP zircon U–Pb geochronology of the plagiogranites from Bayingou ophiolite in North Tianshan Mountains and the petrogenesis of the ophiolite. *Acta Petrologica Sinica*, *22*, 83–94. (in Chinese with English abstract)

Yang, H. B., Gao, P., Li, B., & Zhang, Q. J. (2005). The geological character of the Sinian Dalubayi ophiolite in the west Tianshan, Xinjiang. *Xinjiang Geology*, *23*, 123–126. (in Chinese with English abstract)

Yang, J. S., Xu, X. Z., Li, T. F., Chen, S. Y., Ren, Y. F., Li, J. Y., & Liu, Z. (2011). U–Pb ages of zircons from ophiolite and related rocks in the Kumishi region at the southern margin of Middle Tianshan, Xinjiang: Evidence of early Paleozoic oceanic basin. *Acta Petrologica Sinica*, *27*, 77–95. (in Chinese with English abstract)

Yong, W. J., Zhang, L., Hall, C. M., Mukasa, S. B., & Essene, E. J. (2013). The $^{40}Ar/^{39}Ar$ and Rb–Sr chronology of the Precambrian Aksu blueschists in western China. *Journal of Asian Earth Sciences*, *63*, 197–205.

Zhang, C. L., Li, H. K., & Santosh, M. (2013). Revisiting the tectonic evolution of South China: Interaction between the Rodinia superplume and plate subduction? *Terra Nova*, *25*, 212–220.

Zhang, C. L., Li, H. K., & Wang, H. Y. (2012). A review on Precambrian tectonic evolution of Tarim Block: Possibility of interaction between Neoproterozoic plate subduction and mantle plume. *Geological Review*, *58*, 923–936. (in Chinese with English abstract)

Zhang, C. L., Zou, H. B., Li, H. K., & Wang, H. Y. (2013). Tectonic framework and evolution of the Tarim Block in NW China. *Gondwana Research*, *23*, 1306–1315.

Zhang, J. X., Mattinson, C. G., Yu, S. Y., & Li, Y. S. (2014). Combined rutile–zircon thermometry and U–Pb geochronology: New constraints on early Paleozoic HP/UHT granulite in the south Altyn Tagh, North Tibet, China. *Lithos*, *200–201*, 241–257.

Zhang, L., & Jin, Z. M. (2016). High-temperature metamorphism of the Yushugou ophiolitic slice: Late Devonian subduction of seamount and mid-oceanic ridge in the South Tianshan orogen. *Journal of Asian Earth Sciences*, *132*, 75–93.

Zhang, L., Zhang, L. F., Xia, B., & Lü, Z. (2018). Metamorphic P–T path and zircon U–Pb dating of HP mafic granulites in the Yushugou granulite-peridotite complex, Chinese South Tianshan. *Journal of Asian Earth Sciences*, *153*, 346–364.

Zhang, L. F., Ai, Y. L., Li, X. P., Rubatto, D., Song, B., Williams, S., et al. (2007). Triassic collision of western Tianshan orogenic belt, China: Evidence from SHRIMP U–Pb dating of zircon from HP/UHP eclogitic rocks. *Lithos*, *96*, 266–280.

Zhang, Z. C., Guo, Z. J., & Song, B. (2009). SHRIMP zircon dating of gabbro from the ophiolite mélange in the northern Altyn Tagh and its geological implications. *Acta Petrologica Sinica*, *25*, 568–576. (in Chinese with English abstract)

Zhao, Z. Y., Zhang, Z. C., Santosh, M., Huang, H., Cheng, Z. G., & Ye, J. C. (2015). Early Paleozoic magmatic record from the northern margin of the Tarim craton: Further insights on the evolution of the Central Asian Orogenic Belt. *Gondwana Research*, *28*, 328–347.

Zhong, L. L., Wang, B., Shu, L. S., Liu, H. S., Mu, L. X., Ma, Y. Z., & Zhai, Y. Z. (2015). Structural overprints of early Paleozoic arc-related intrusive rocks in the Chinese Central Tianshan: Implications for Paleozoic accretionary tectonics in SW Central Asian Orogenic Belts. *Journal of Asian Earth Sciences*, *113*, 194–217. https://doi.org/10.1016/j.jseaes.2014.12.003

Zhu, W. B., Zheng, B. H., Shu, L. S., Ma, D. S., Wu, H. L., Li, Y. X., et al. (2011). Neoproterozoic tectonic evolution of the Precambrian Aksu blueschist terrane, northwestern Tarim, China: Insights from LA-ICP-MS zircon U–Pb ages and geochemical data. *Precambrian Research*, *185*, 215–230.

Zhu, Y. F., Guo, X., Song, B., Zhang, L. F., & Gu, L. B. (2009). Petrology, Sr–Nd–Hf isotopic geochemistry and zircon chronology of the late Palaeozoic volcanic rocks in the southwestern Tianshan Mountains, Xinjiang, NW China. *Journal of the Geological Society*, *166*, 1085–1099.